3-D Numerical Simulation and Analysis of Complex Fiber Geometry RaFC Materials with High Volume Fraction and High Aspect Ratio based on ABAQUS PYTHON

BY BoCheng Jin

A thesis submitted to the

Graduate School—New Brunswick

Rutgers, The State University of New Jersey

in partial fulfillment of the requirements

for the degree of

Master of Science

Graduate Program in Mechanical and Aerospace Engineering

Written under the direction of

Professor Assimina Pelegri

and approved by

____

____

____

____

New Brunswick, New Jersey

May, 2011

ABSTRACT OF THE THESIS

3-D Numerical Simulation and Analysis of Complex Fiber Geometry RaFC Materials with High Volume Fraction and High Aspect Ratio based on ABAQUS PYTHON

by BoCheng Jin

Thesis Director: Professor Assimina A. Pelegri

Organic and inorganic fiber reinforced composites with innumerable fiber orientation distributions and fiber geometries are abundantly available in several natural and synthetic structures. Inorganic glass fiber composites have been introduced to numerous applications due to their economical fabrication and tailored structural properties. Numerical characterization of such composite material systems is necessitated due to their intrinsic statistical nature, which renders extensive experimentation prohibitively time consuming and costly. To predict various mechanical behavior and characterizations of Uni-Directional Fiber Composites (UDFC) and Random Fiber Composites (RaFC), we numerically developed Representative Volume Elements (RVE) with high accuracy and efficiency and with complex fiber geometric representations encountered in uni-directional and random fiber networks.

In this thesis, the numerical simulations of unidirectional RaFC fiber strand RVE models (VF>70%) are first presented by programming in ABAQUS PYTHON. Secondly, when the cross sectional aspect ratios (AR) of the second phase fiber inclusions are not necessarily one, various types of RVE models with different cross sectional shape fibers are simulated and discussed. A modified random sequential absorption algorithm is applied to enhance the volume fraction number (VF) of the RVE, which the mechanical properties represents the composite material. Thirdly, based on a Spatial Segment Shortest Distance (SSSD) algorithm, a 3-Dimentional RaFC material RVE model is simulated in ABAQUS PYTHON with randomly oriented and distributed straight fibers of high fiber aspect ratio (AR=100:1) and volume fraction (VF=31.8%). Fourthly, the piecewise multi-segments fiber geometry is obtained in MATLAB environment by a modified SSSD algorithm. Finally, numerical methods including the polynomial curve fitting and piecewise quadratic and cubic B-spline interpolation are applied to optimize the RaFC fiber geometries. Based on the multi-segments fiber geometries and aforementioned techniques, smooth curved fiber geometries depicted by cubic B-spline polynomial interpolation are obtained and different types of RaFC RVEs with high fiber filament aspect ratio (AR>3000:1) and high RVE volume fraction (VF>40.29%) are simulated by ABAQUS scripting language PYTHON programming.

Acknowledgements

First I want to express my gratitude to my advisor Prof. Assimina A. Pelegri, for holding my hand and introduced me into this research field. It has been a great pleasure to work with her; all the directions she gave me turned out to be very interesting research efforts. I will always be grateful for the learning opportunities she has provided me, and for her kindness and encouragements.

I wish to express appreciation to my mentor Prof. Ellis H. Dill, who has been teaching me with unbelievable patience on Finite Element Methods. His style influenced me a lot in a good way. We worked together on his new book <<The Finite Element Method for the Mechanics of Solids>>, its <<Solution Manual>>, on his graduate level course "Computational Solid Mechanics" and on his undergraduate level course "Airplane Structures". Grandpa Dill has truly taught "Twiddle Finger" everything, not only academically, but also how to be a righteous man.

My appreciations to Dean Jeffrey L. Rankin of the School of Engineering, to Graduate Director Prof. Haim Baruh and Prof. William J. Bottega, to Undergraduate Director Prof. Hae Chang Gea of the Mechanical and Aerospace Engineering Department, for awarding me the Undergraduate Course Instructor Positions for fourteen times, the Teaching Assistant Fellowships for two years, the Undergraduate Teaching Aid Positions for two times during my master degree study. It was a pain in the neck to teach all those freshman courses, but lots of fun.

My best wishes and appreciation to my undergraduate thesis advisor, Chair and Prof. Jürgen Wilde of IMTEK in University of Freiburg in Germany, you are always the best. To the establisher of my wonderful memories: my colleagues and my best friends Dr. Johan Dalin and Dr. Thomas Fellner.

To my dearest mom and dad, who have always persuaded me to pursue my dreams and have made enormous sacrifices and efforts to make this real. I could not have done any of these without your boundless love and encouragements.

Dedication

To my mom, Y. Zhang.

Table of Contents

Chapter 1

Introduction

In view of the increasing demand in aerospace and automotive industries for cheaper materials with lower density and superior strength to weight and modulus to weight ratios, fiber reinforced composites (FRC) have been introduced to numerous applications due to their supreme strength and stiffness properties along with their lightweight characteristics [1-5]. However the cost of traditional FRC materials is still considerable. Random chopped fiber reinforced composites (RaFC) have become a promising alternative for their low cost; light weight structure, and efficient production capability [5]. To obtain RaFC materials with better mechanical and physical behaviors, the traditional experimental methods have been explored but yet to be extremely resource and time consuming. In the last four decades the finite element methods (FEM) have successfully become a prevalent computational analyzing technique of designing RaFC materials with optimized physical properties [6]. In order to apply FEM and accurately predict different types of RaFC materials' various behavior and characterizations, such as 2D and 3D static and dynamic stress, deformation analysis, fatigue strength and stability, joint design and laminate sizing, impact and crashworthiness, fracture toughness and delamination problems [7, 8], it is vital to numerically establish accurate RaFC material simulation models and obtain their effective characterizations. The main difficulty in this step lies in modeling true

RaFC fiber geometries at high fiber filament aspect ratio (AR>20:1) and high fiber volume fraction number (VF>20%). In this thesis, various FRC models with true smooth curved fiber geometries and high AR (AR>3000:1 for RaFC), high VF (VF>70% for Uni-Directional UDFC, VF>40.29% for Random Directional RaFC) will be presented.

The RaFC materials consist of high strength fibers embedded in or bonded to a matrix with distinct interfaces or boundaries in between. This combination gives superior performance compared to the properties of the individual components. The principal load-transferring medium matrix material is thermosetting epoxy resin polymer, metal, or ceramic [6], which keeps the fibers in the desired location and orientation while protecting them from environmental damages. The principal load-carrying RaFC fibers in commercial and industrial use are various types of glass and carbon fibers in the form of either continuous long fibers at the approximate length of 50mm, or discontinuous short fibers at length ranges from 0.5mm to 6mm [6, 9]. Fibers lengths are controlled by cutting or chopping either during or after production and are therefore independent of the forming processes [10].

Fiber diameters, however, various a wide range due to different manufacturing processes and has important effects on overall material behaviors thus need to be taken into consideration for measurement and testing. E. Cendre et al. [11] used high resolution x-ray synchrotron micro-tomography to measure two samples of unidirectional glass-fiber composite material with VF of 55% and reported 3D computerized tomography (CT) images, which demonstrated the irregular fiber distribution and the varying glass fiber diameters range from 0.0102mm to 0.0234mm at an average diameter of 0.0156mm. The commercial and industrial use carbon fibers have diameters in the range of [0.0050mm, 0.0100mm] [10]. Y. Fang [12] experimentally investigated the diameters effects associated with single glass-fiber filaments strength and with glass-fiber composite bending strength, and determined that the average strengths of single glass fiber filaments decrease from 2.52×10^3MPa to 1.81×10^3MPa as their average diameters increase from 0.0136mm to 0.0298mm. In contrast, the bending strengths of dry-state glass fiber composites reduced from 1070MPa to 848Mpa with an average glass fibers diameter reduction from 0.023mm to 0.008mm. Glass-fibers which are finer than about 0.006mm become both physically and economically difficult to pull. Very high strength glass fiber reinforced material composites have fiber diameters of about 0.001mm but are yet not easy to be manufactured.

It is important to have background knowledge about how a representative volume element (RVE) model, on which FEA will be performed, is identified and generated. The identification of a RVE is obvious in laminate and woven composite materials [13][14] due to the repeatable structure of the architecture. However, in composite materials with random fiber reinforcements the numerical simulation of an RVE is not straightforward. Similar to the RVE definition of those composites that have repeatable structure the RaFC RVE, of which the fiber reinforcement inclusions have random orientation distribution and location, additionally requires a statistical representation of its characteristics. When generating an RVE, the geometry shapes of the second phase fiber reinforcements are generated in a fixed volume box and follow certain rules such as location and orientation distribution predefined and physically non-collision. In this thesis, the fiber reinforcements are recognized as second phase and different types of FRC RVE models (e.g. Uni-directional single fiber strand RVE; RaFC RVE) are being generated and analyzed.

There are five key methods that have been used for numerical generation of composites materials' RVEs, namely, molecular dynamics method; Voronoi tessellation scheme [22]; Monte Carlo procedure (mechanical contraction method); random sequential adsorption (RSA) method [25, 33]; and image reconstruction technique. One of the earliest methods had been used was based on molecular dynamics using an equilibrium fluid as a starting point. The shortcomings of this method were pointed by Williams and Philipse [15], that when two fibers approaching each other dominantly due to their own expansion rather than their thermal velocities, an elastic collision will result in a postcollision separation rate between the two fibers centers, which is less than the rate at which the fibers are expanding. This will result in the pair of fibers' physical interfere with each other. Another novel method used by Hinrichsen et al [16] was to form a Voronoi tessellation around amount of reinforcements, which are all then moved to the center of their Voronoi cell and the RVE volume is reduced as much as possible until a pair of fibers came into contact with each other. The procedure is repeated until the RVE could no longer be reduced in volume.

Related to the Voronoi tessellation method, Monte Carlo (MC) simulations have been widely used in RVE generation. The MC two-step procedures start with a configuration with arbitrary fiber reinforcement locations and orientations within a large box, and rearrange their locations and orientation without accepting physical intersections, until the predetermined desired orientation state is reached. At the end of the procedure, the size of the large box is decreased toward the designated fiber volume fraction without altering the orientation of the fibers. The MC method has been widely used by Gusev and his coworkers [17-19] for studying the material properties of short fiber FRCs.

The random sequential adsorption (RSA) [25,33] schemes were very popular in studying particle packing and generating FRC RVEs for spheres [20-23], spherocylinders [20,22], ellipsoids and rods [20-22,26]. During RSA reinforced fibers are added to the RVE region by randomly generating its location and orientation angle. The new fibers to be generated can not intersect with any of the previous generated ones. Boehm et al [20] applied the modified RSA method and achieved 15% volume fraction (VF) in generating metal matrix composites RVEs with random short fibers of aspect ratio AR=5. Fiber reinforcements are not allowed to overlap in RSA thus a minimum distance between any two fibers is set with regard to the side length of the RVE model. Geometrical periodicity is usually applied with RSA scheme to enhance the volume fraction number (VF). Tu et al. [21], Iorga et al. and Pan et al. [24] applied modified RSA algorithm and achieved RVE with AR=7 for spherical particles and AR=10 (with VF=13.5%) for random glass chopped fibers, respectively. It was noted that the VF achievable through RSA is much smaller than that predicted by existing analytical models and Widom [25] refers to the phenomenon as “Jamming Effect”. To overcome the jamming effect, Kari et al. [26] used different sizes of fibers by depositing them inside the RVE in a descending manner. The largest aspect ratio fibers are first deposited and when reaching the jamming limit, thee next largest possible aspect ratio fibers in the RVE are generated. This method is also used in this thesis when generating RVE for single fiber strand in the RaFC material.

A resent new method applied in RVE generation is the 3D image reconstruction via X-ray tomography and image processing technique. Some good examples on glass fiber reinforcement polymers (FRPs) and wood fiberboard based on the CT tomographic image reconstruction are presented by Redenbach et al. [27] and Faessel et al. [28]. The 3D fiber networks of the samples are reconstructed and generated based on X-ray absorption radiographs using specialized software. However such method for generating numerical representations of FRCs disadvantageous in that the obtained geometries can not be modified for different composite architectures for achieving better material properties, which limited its appeal.

While the 3D CT application appears attracting for the random fiber networks, modeling of composites with straight fibers of fixed aspect ratio using Monte Carlo and RSA procedures [25, 33] were found to be reaching low fiber volume fractions. When the fibers are modeled as short straight cylinders with small AR lower than 10, the VF of the RVE is generally found to be less then 25%. For fibers with AR 20, the relation between the fiber AR and the maximum achievable fiber VF was 20% as illustrated by Evans et al. [29], 30% by Parkhouse et al. [30], 18.5% by Toll et al. [31], and 27% by Williams et al. [22]. However, their results not only indicated that the increase of the fiber aspect ratio will result in decrease of the maximum achievable fiber volume fraction, but also the volume fraction as predicted by their RVE models are still relatively small compared to the composites used in industrial applications which have volume fractions larger than 40% [24,32].

Modeling RaFC materials with high fiber filament aspect ratios (AR>20:1) and high fiber volume fractions (VF>20%) in PYTHON scripting is challenging. Nevertheless, the PYTHON scripting language can not only access ABAQUS model databases to automatically establish complex geometries and apply materials properties in its CAE modulus, but - more importantly - is also able to merge FEM procedures within the programmed codes and perform FEA tests in ABAQUS Standard/Explicit automatically. In this thesis, different types of FRC RVEs, for example, different Uni-directional FRC RVEs with various types of fibers and with VF>70% (in ABAQUS PYTHON); 3-D random fiber composites RaFC RVEs with straight cylinder fiber filaments of AR=100:1 and VF>31.8% (in ABAQUS PYTHON); piecewise multi-segments fiber geometries RVEs (in MATLAB); 3-D random fiber composites RaFC RVEs with B-Spline interpolated smooth curved fiber strands with AR=3000:1 and VF>40.29% (in ABAQUS PYTHON), are simulated for illustration purpose by taking the advantage of PYTHON scripting language programming and the automatic complex geometries generation in ABAQUS and MATLAB.

Chapter 2

Experimental Observation and Numerical Simulation of RaFC material Fiber Strand RVEs

A typical E-glass fiber reinforced in a polyurethane matrix random fiber composite (RaFC) specimen is illustrated in Fig 2-1. In order to simulate real RaFC material geometry and for properties testing purpose, observation on the material specimen and their accurate texture data are required as the first important step.

The RaFC material specimen consists of random distributed fiber strands, which can be observed and measured clearly from the top view of the specimen in Fig 2-1. By measurements from top view, these randomly distributed fiber strands are statistically 50mm (approximately 2 inches) in length and 1mm in width. The cross section shape of the fiber strands needs to be discussed upon the experimental observations.

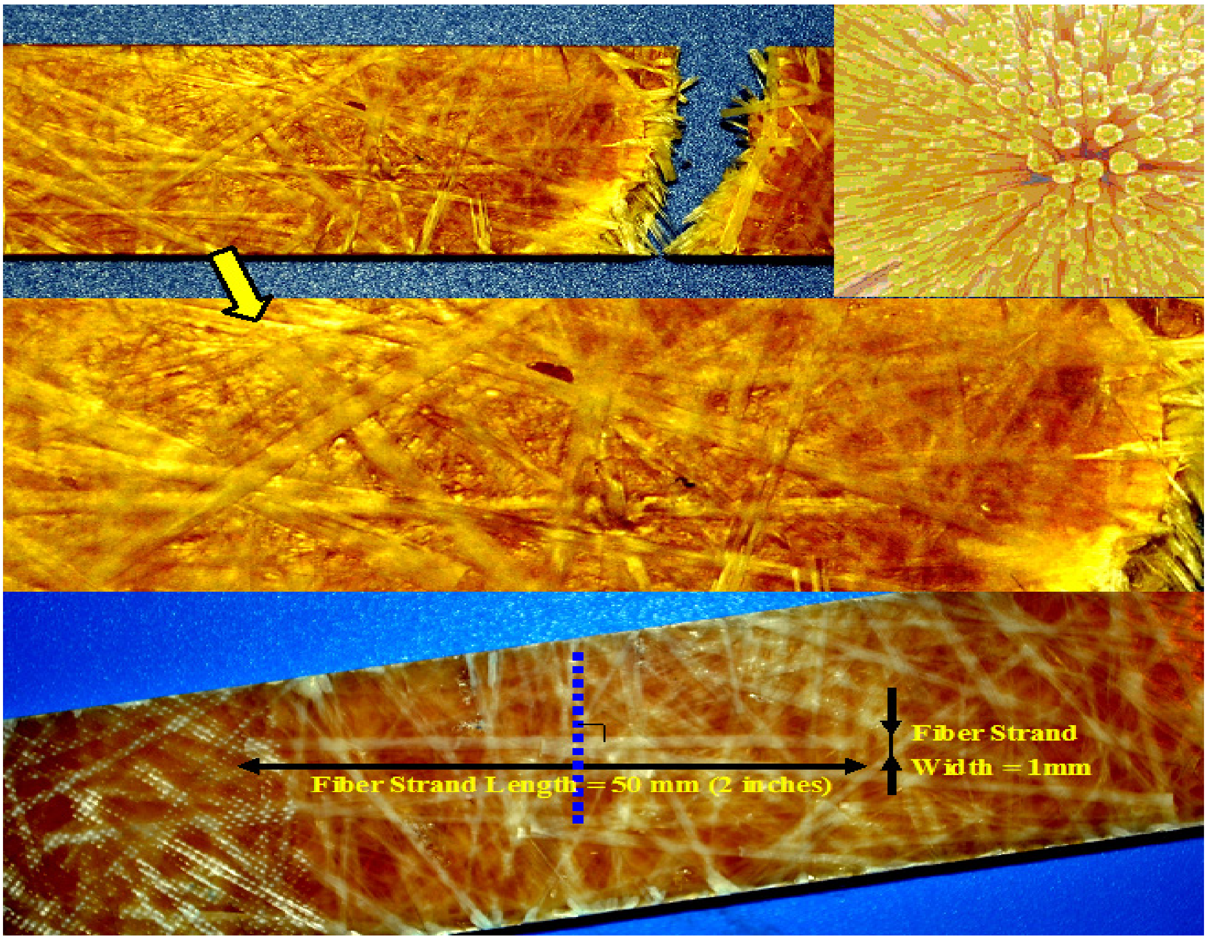

Fig 2-1. A RaFC material specimen. Note that a fiber strand is identified by the black line segment with arrows, blue dash line segment shows a later performed cut, which is perpendicular to the strand longitudinal direction. Top right corner shows a 3D XTM view of a unidirectional glass-fiber strand with fiber volume fraction of 55%.

Various experimental works have been done in observing the microstructure of RaFC materials via optical or electron microscope and scanner. However the characteristics of the composites were found to be easily altered during the necessary surface preparation for the microscope studies, due to unavoidable damage and removal of fiber filaments in the strands during the process of cutting and polishing of the specimen, as shown in Fig 2-2.

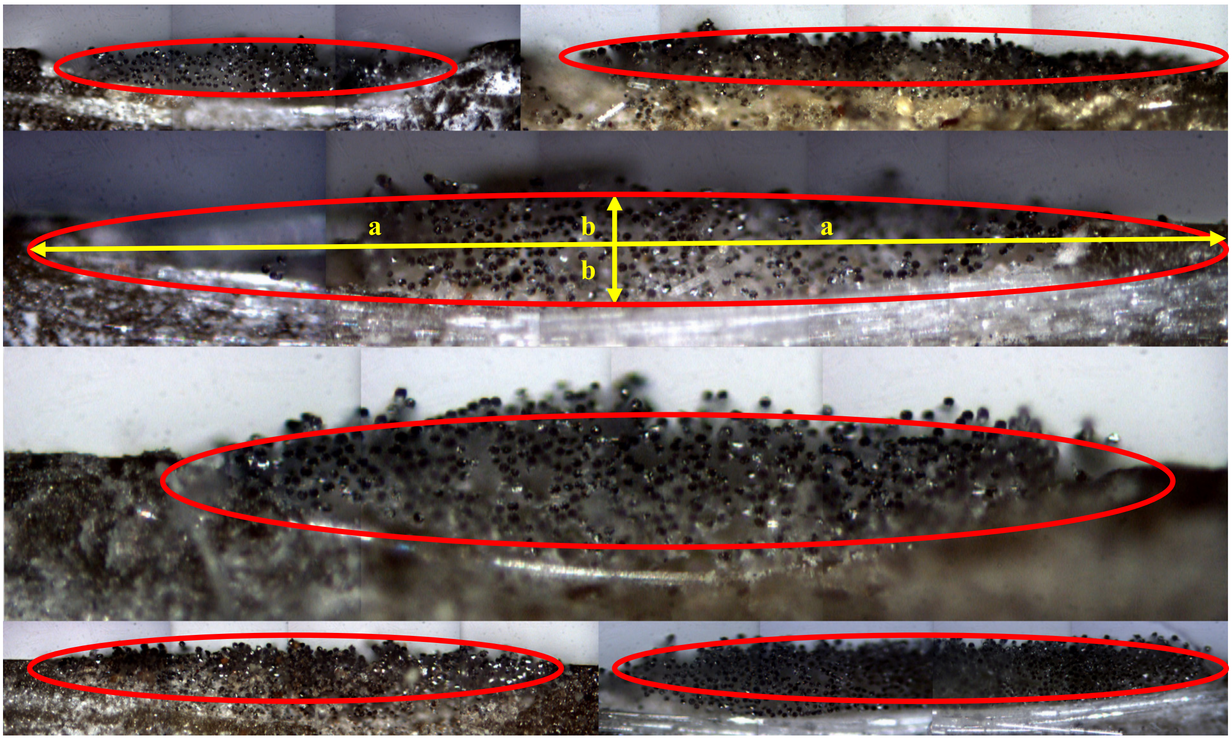

Fig 2-2: An electron microscope image of RaFC material fiber strand cross section. Specimen preprocessed by cutting and polishing. Note the damage and removal of fibers on the left corner of the elliptical cross section.

To avoid this disadvantage, Cendre and Feih et al. [11] recently applied the X-ray tomographic microscopy (XTM) as a non-destructive characterization technique, which not only provides direct high resolution images of the heterogeneous materials bulk but also enabling the distinction of individual fibers and matrix in composites. As a result, the irregular fiber distribution and varying fiber diameters are easily detected in high resolution XTM. On top right corner of Fig 2-1 shows a 3D XTM view of a unidirectional E-glass composite specimen with 55% fiber volume fraction. The cross section (c/s) perpendicular to the fiber not only elucidates the irregular fiber distribution but also clearly indicates the varying fiber diameter dimensions.

In order to accurately represent the geometry of the specimen to be simulated, and since the debonding of a whole fiber strand is not easily achievable, cross sections (c/s) perpendicular to the longitudinal direction of the fibers strand are examined with a scanning electron microscope (SEM) and appear to have elliptical configurations, as shown in Fig 2-2. The semi-major axis length of the cross section ellipse is defined as "a" and the semi-minor axis length of the cross section ellipse is defined as "b". Note that the major axis of the cross section ellipse, which in Fig 2-2 as the length "$2a$", is identical with the 1mm fiber strand width shown in Fig 2-1.

Multiple perpendicular cuts with high precision and observation on the cross sections were performed. The cross sections texture parameters of the fiber strand were measured statistically. The average semi-minor axis length of the cross section (c/s) ellipse is statistically determined as 0.03mm; while the average semi-major axis length of the cross section (c/s) ellipse is 0.50mm resulting in fiber c/s aspect ratio of $2a/2b$ = 16.67:1.

Based on the aforementioned observation, each fiber strand (identified by black line segment with arrows in Fig 2-1) of the RaFC can be modeled as an elliptical cylinder. The normalized texture parameters of one fiber strand geometry are summarized proportionally as follows: the cross section shape of the fiber strand is an ellipse with semi-major axis length of "a" and semi-minor axis length of "b", cross sectional aspect ratio of the ellipse $2a/2b$ =16.67:1. The length of the fiber strand (elliptical cylinder) equals to $100a$, the width of the fiber strand equals to $2a$. All fiber filaments are unidirectionally aligned along the longitudinal direction of each fiber strand.

The information of single fiber filaments inside the fiber strands is also required throughout the simulation. Fig 2-2 shows that each fiber strand has a VF of more than 60% and contains thousands of single fiber filaments. The cross sections of these fiber filaments are experimentally identified as circular shape and their radiuses are measured and range from 0.010mm (10μm) to 0.025mm (25μm), with an average radius of 0.016mm (16μm). All single fiber filaments are unidirectionally aligned along the longitudinal/axial direction of each fiber strand. This configuration is known as unidirectional FRC material which has high stiffness and high strength along the longitudinal/axial direction of the fiber strand. The effective elastic properties of this two-phase FRC material are dependent on elastic properties of their constituents as well as the micro-geometry of the fibers which is acting as the reinforcing phase. Jones et al [34], Ramsteinera et al [35], Miwa et al [36], showed that different material configuration parameters such as fiber diameters, fiber length, fiber volume fraction number, and fiber distribution throughout the composite material, all play crucial roles for certain composites mechanical properties such as material strength and Young's modulus. Moreover, in contrast to the circular cross section (c/s) fiber filament reinforcements, Zhao et al [37] derived the elastic moduli in terms of the c/s aspect ratio and the fibers volume fraction, while the cross sectional aspect ratio approaches zero and the fibers exist as thin elliptical ribbons. The analysis theoretically indicates that fibers with elliptical c/s (ribbon shape fibers) are far more effective in terms of mechanical properties than the traditional circular cylinder fiber filament reinforcement.

In order to capture the characteristics of the real material structures observed above, a 3D RaFC fiber strand RVE (Representative Volume Element) model needs to be generated automatically. Based on PYTHON (ABAQUS scripting language), analytical geometry algorithms are developed to establish the fiber strand RVE material model which is related to the mentioned accurate experimental work. The random sequential adsorption/addition (RSA) scheme is applied. Fiber collision and interpenetration was not permitted throughout the process as reflected throughout the protocol, which is summarized in *Section 2.1*. The collision detection algorithms and a modified RSA scheme are applied to enhance the volume fraction of the RVE model and are discussed in *Section 2.2*. Finally in *Section 2.3*, a spatial segment shortest distance (SSSD) algorithm is developed based 3D space analytical geometry and a RaFC RVE model in 3D space is simulated.

2.1. Numerical Modeling of a Single RaFC Fiber Strand RVE by RSA.

The term Data Structure in PYTHON language is referred as the term Dictionary, the Array is referred as the term List. The tree data structure is applied throughout the algorithm. The RVE List includes multiple “FIBER” dictionaries (each “FIBER” dictionary includes integer, or float variables and matrices such as fiber-number; fiber-volume; fiber-translate-matrix; fiber-rotation-matrix), and sub-dictionaries (such as fiber-type-dictionary, segment-dictionary).

Two sub-dictionaries are illustrated here as examples:

(a) fiber-type-dictionary, which includes a cylindrical-fiber-filament-dictionary with a final sub-dictionary of the cross sectional radius "*r*", and an elliptical-fiber-filament-dictionary with a final sub-dictionary of semi-major axis "*a*" and semi-minor axis "*b*"

(b) segment-dictionary, encompasses variables such as segment-number; part-name; instance-name; layer-number; and last level sub-dictionary like segments-end-points. The last level sub-dictionary segments-end-points are defined as spatial Cartesian coordinate points: $\{'x_1','y_1','z_1'\}$ and $\{'x_2','y_2','z_2'\}$.

The fiber filament lengths are identical in one fiber strand and are controlled by cutting or chopping either during or after production therefore are independent of the forming processes. A cross section perpendicular to the fiber strand longitudinal direction is considered as fiber strand RVE model. In order to overcome the jamming difficulty in generating a time effectively RVE with a high fiber volume fraction number, a value of $50{\times}r$ is set as the side length of the squared shape RVE. In what follows, the protocol to generate the fiber strand RVE is described.

(1). At the beginning of each iteration, a fiber filament with either circular c/s of radius "*r*", or with elliptical c/s of semi-major axis "*a*" and semi-minor axis "*b*", is generated along z-axis in ABAQUS.

(2). A random rotation matrix is generated and applied to the *current* fiber filament. Note that the current fiber along the z-axis will be randomly rotated about z-axis only.

(3). A random translation matrix is generated and applied to the *current* rotated fiber filament. Note that the current fiber will be translated within x-y plane only.

(4). The *current* fiber is filtered with the compatibility collision detection algorithm (*Section 2.2*). If any physical collision of the *current* fiber filament with existing local ones is detected, the *current* fiber will be either moved to the vacant space and go through the iteration procedure until generated, or will be simply discarded if overflow. Otherwise, the examined fiber filament will be generated at this new collision free position.

(5). If the fiber filament is successfully generated, its volume will be calculated and added to the current total fiber volume within the RVE.

(6). At the end of each iteration, the current total fiber volume fraction is calculated and compared to the requested volume fraction. The algorithm will continue unless it meets with either of the following two conditions: the current fiber volume fraction reaches or exceeds the requested volume fraction value; or when additional attempts are do not provide any meaningful improvements, that is the total iteration number overflows or exceeds a preset experience based value.

(7). RVE is successfully generated. Calculate and output all necessary parameters, such as relations between nearest neighbor separation distance to each kind of fiber filament, the statistic results of volume fraction number to different fiber textures, fiber quantities conclusion to different fiber textures, etc.

2.2. A Modified RSA Scheme with Collision Detection Algorithm

Since all fiber filaments are unidirectional aligned thus the collision situation does not vary along z axis, only the cross section of the RVE on x-y plane needed to be checked for fiber collision detection. In order to increase the efficiency of the algorithm, the RVE is divided into 625 second level sub-squares with each side length of $2\times r$, as shown in Fig 2-3. When the center point of the newly introduced fiber filament is located on the edge of any second level square, filament collision check is preformed to the fibers filaments located within up to four (4) neighboring squares, as shown in the blue region in lower right corner of Fig 2-3. When the center point of the newly introduced fiber filament is located within a certain second level square, the collision check of this fiber filament is preformed to the filaments located within to eight (8) second level squares around the current location, as shown in the green region in top left corner of Fig 2-3.

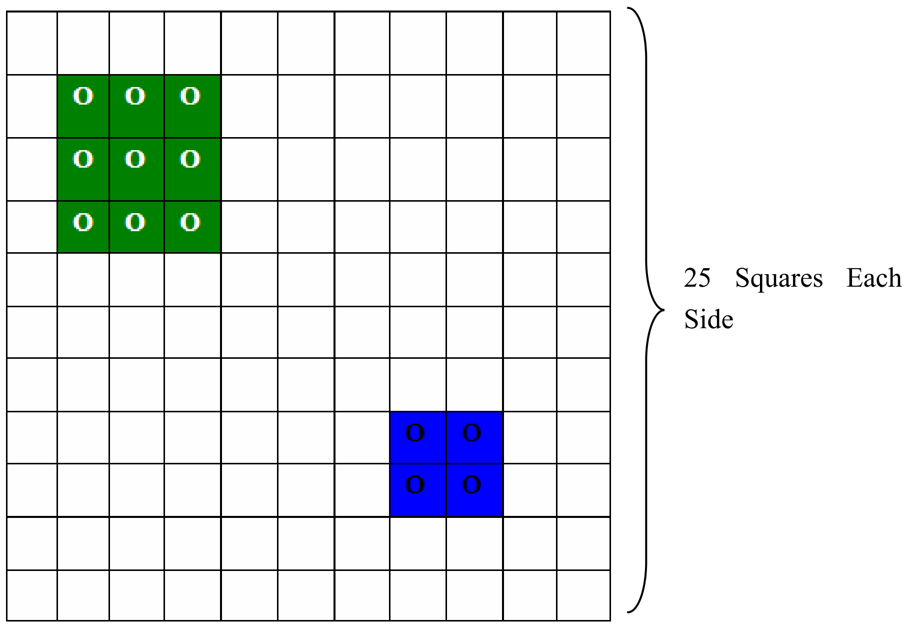

Fig 2-3. RVE spatial division.

Geometry compatibility test is performed between any two fiber filaments that are required to be checked for physical collision. Two different types of fiber filament geometry are discussed in this thesis, namely circular and elliptical cross section.

2.2.1 Circular Cross Section Fiber Filaments

In the previous considerable studies on unidirectional FRC materials, the filament cross section has been treated as circular shape. For circular cross section fiber filaments, the calculated x-y plane distance from the new filament's center position to the center position of existing filament, should fit the following criterion:

$$d_{criterion} <= 2 \times r + d_{\min} \tag{2-1}$$

where $d_{\min}$ is the preset minimum tolerable distance between any two fiber filaments and r is the filament's radius. These two fibers are either overlap with each other or they are too close to each other thus do not meet the requirement. In this case, the new generated fiber will be discarded. Otherwise, a new fiber will be generated based on the new collision free position.

Followed the collision detection criterion, a unidirectional RVE model of RaFC fiber strand is generated and presented in Fig 2-4(a), with the fiber volume fraction number of 60%. Each fiber filament has the same radius "*r*" and aspect ratio of *l/r* = 100:1 (*l*: fiber filament length). Additionally, by applying a proper boundary conditions the real fiber strand configuration in the RaFC specimen can be achieved as shown in Fig 2-4(b) and Fig 2-4(c). The shape of the RVE is described by the canonical implicit elliptical equation:

$$\frac{x^2}{a^2} + \frac{y^2}{b^2} < 1 \tag{2-2}$$

According to the experimental observation in the previous section, the radiuses of the fiber filaments are however obviously not identical. Fiber filaments radiuses in RaFC material range from 0.010mm (10μm) to 0.025mm (25μm), with an average radius of 0.016mm (16μm). Based on this fact, the RSA algorithm is modified and the collision detection criterion of the cylindrical fibers is expressed as:

$$d_{criterion} <= r_1 + r_2 + d_{\min} \tag{2-3}$$

note that r_1 and r_2 are the filament radii involved in the collision detection.

While the fiber filaments radii can vary, the volume fraction number of the RVE may theoretically reach 100%. A RVE model consists of fiber filaments with a variety of radii is presented in Fig 2-4(d) and Fig 2-4(e), with volume fraction of 65% and 70% respectively.

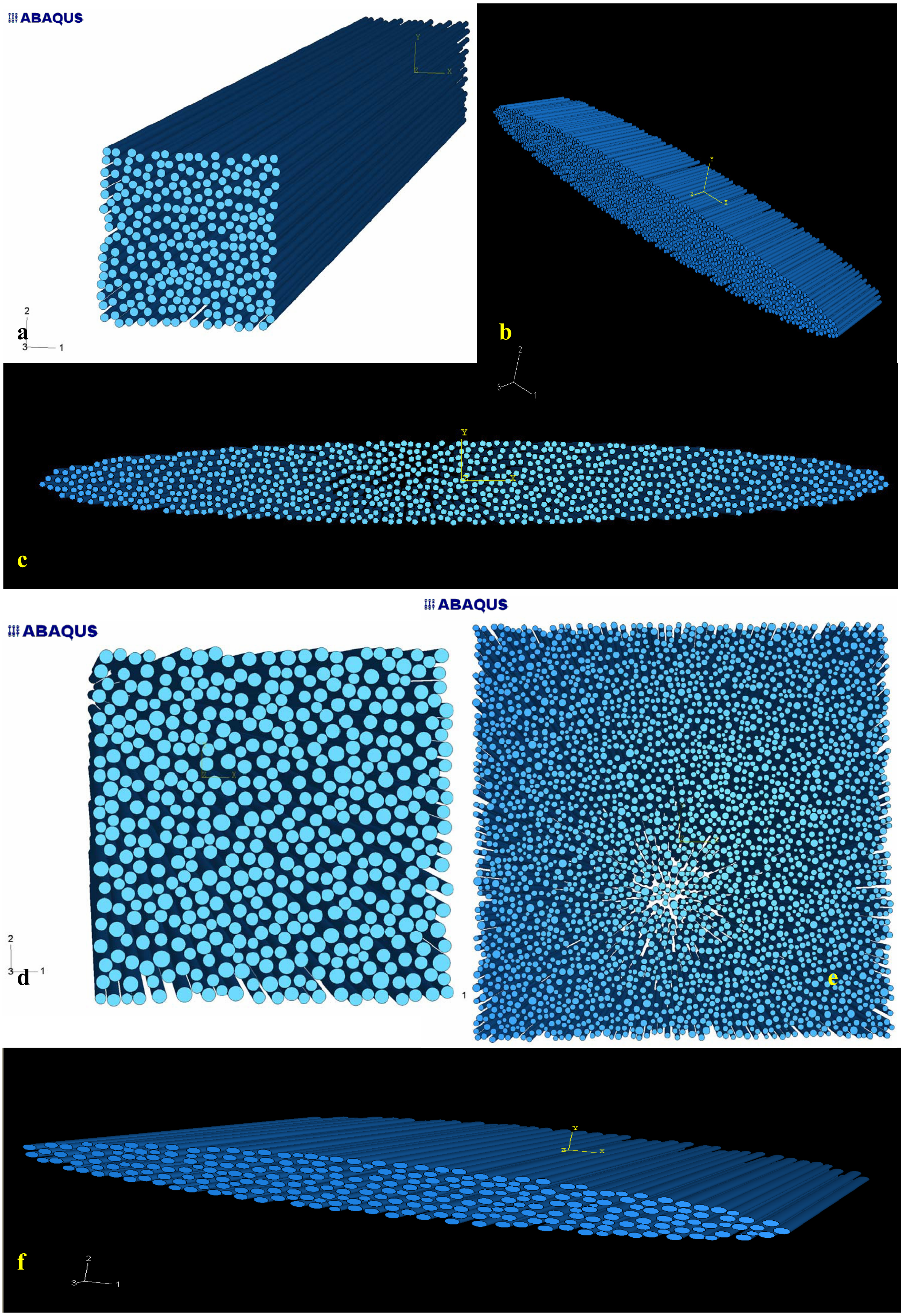

Fig 2-4. Unidirectional fiber strand RVEs

2.2.2 Elliptical Cross Section Fiber Filaments

The shape of the fiber filaments cross sections are however not necessarily to be circular. When the fibers exist in the form of elliptical cylinders such that the aspect ratio *a/b* of the cross section (thickness to width ratio) is not one, the moduli of the fiber, thus the composite, will be different since elliptical filaments present higher packing capacity as well as more anisotropy. Especially when the aspect ratio approaches zero, the reinforcing fibers become ribbons and are being able to be easily processed and will have great potential applications if the calculation results of composite properties are superior to that reinforced with circular fibers.

In this RVE, the fiber filament's elliptical c/s, see Fig 2-5, is defined as a set of points (X, Y) of the Cartesian plane that satisfy the implicit ellipse equation:

$$AX^2 + BXY + CY^2 + DX + EY + F = 0, \tag{2-4}$$

provided that $B^2 - 4AC < 0$. Two collision detection algorithms are proposed.

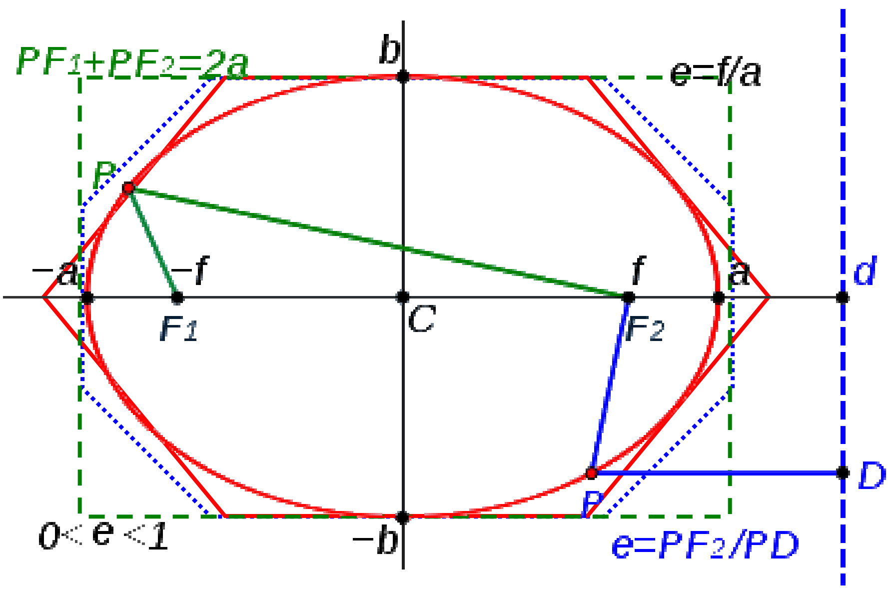

Fig 2-5. The Polygon method for elliptical cross sectional fiber reinforcement

2.2.2.1 Algorithm 1 - Polygon method: Since the semi-major axes of ellipses are always parallel to the x-z plane, polygons are applied to approach and replace the elliptical cross section for collision detection purpose. In this polygon collision detection algorithm, two ellipses are considered as "collision free" if the two polygons surrounding them are not interfere with, or included in, one another. The detection of two polygons can be reduced to the collision detection of the polygons' edges. So as to avoid the situation in which one polygon included by another, two points in each polygon are picked randomly and tested to see if they exist in both polygons. Fig 2-5 illustrates the elliptical c/s as approximated by a square; a hexagon; and an octagon.

During execution of the polygon method, the algorithm's efficiency heavily depends on the ellipse's cross sectional aspect ratio *a*/*b;* in particular when *a*/*b* approaches zero, that is, ribbon shaped filaments, the packing efficiency is increased. Furthermore, employment of the polygon method results in overall reduction of the fiber volume (VF) in the RVE since the available space for generation of new fibers is limited. For instance, in the case of approximating a circular c/s filament (a/b=1) using a rectangular polygon the maximum volume fraction is $\frac{\pi}{4}$=78.54%.

2.2.2.2 Algorithm 2 - Minimum collision distance method: The minimum acceptable distance between two elliptical fibers cross section is calculated according to Fig 2-6. In Fig 2-6, the green ellipse represents an existed fiber with center point O_A. The red ellipse with center point O_B represents the current introduced fiber that is required to be checked for collision compatibility. The critical value of collision distance is presented as distance O_AO_C between the green and blue ellipses and calculated according to 2-D analytical geometry; note that O_AO_C includes a minimum tolerable distance between any two elliptical fibers. The collision criterion therefore is obviously described as $O_AO_B>O_AO_C$. New elliptical fiber will be generated when this collision criterion fits, or, will be discarded otherwise.

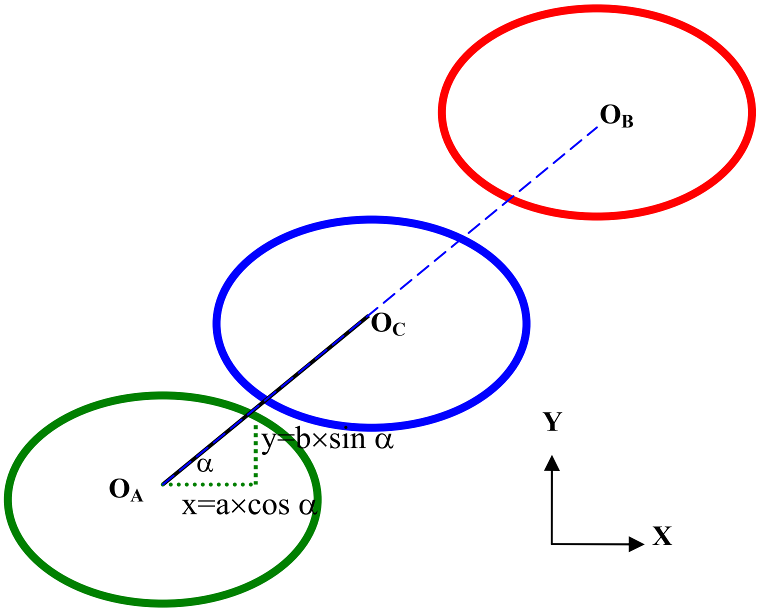

Fig 2-6. Collision detection of elliptical fiber reinforcement

Figure 2-4-(f) illustrates a fiber generated using the algorithm-2, the minimum collision distance method and RVE shape boundary condition as $\frac{x^2}{a^2}+\frac{y^2}{b^2}<1$.

2.3. Numerical Modeling of Cylindrical Reinforced Fiber RaFC RVE.

Based on the aforementioned technique, a Spatial Segment Shortest Distance (SSSD) algorithm is developed by PYTHON (ABAQUS scripting language) and applied in simulating RVEs of random chopped fiber reinforced composites (RaFCs). The flowchart of the process is depicted in Fig. 2-7.

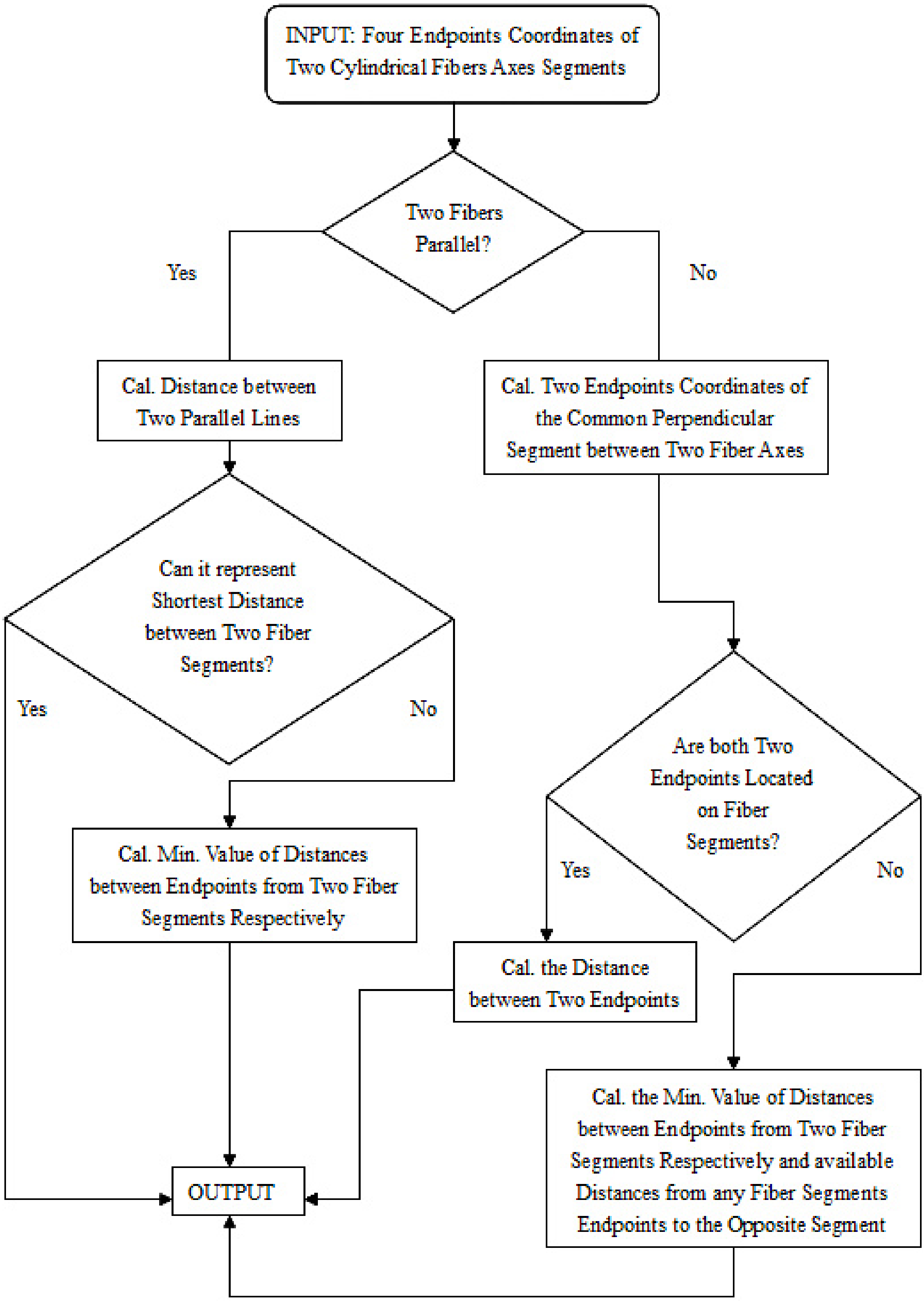

Fig 2-7 Flowchart of SSSD algorithm.

The SSSD algorithm calculates the 3D shortest distance between any two random and limited length segments in space. When calculating the coordinates of two endpoints on the common perpendicular segment between two fibers axes, the cylindrical fiber with circular c/s is defined algebraically as the solution sets of a linear system. For the n^{th} new fiber in the RVE, *n-1* calculations need to be performed with every existed fiber, that is:

$$Ax < b \tag{2-5}$$

where ***A*** is a real 3n×3n matrix, ***b*** is a real 3n×1 vector and ***x*** is a 3n×1 vector including the information of 3D spatial point coordinates of each pair of fibers to be tested. Note that when the current fiber is the 10^3 in sequence, the coordinate vector ***x*** may reach the order of 10^4 and the element number of matrix ***A*** is at the order of 10^6. To optimizationally solve the linear system, a modified LU decomposition algorithm in presence of pivoting is applied:

$$P_{n-1}....P_2P_1AQ_1Q_2....Q_{n-1} = A' \tag{2-6}$$

The system then can be concluded as mentioned:

$$A' = PAQ \tag{2-7}$$

where ***P*** and ***Q*** are the permutation matrices and both have the properties of symmetric and orthogonal, this can be rewritten as:

$$PAQQ^T X < Pb \tag{2-8}$$

The numerical solution of the linear system is then obtained by applying LU decomposition on the new system with **A'** matrix**:**

$$LUx' < b' \tag{2-9}$$

The 3D collision criterion of the fibers is similar to the introduced 2D unidirectional fiber strand simulation: when the shortest distance between any two spatial fibers is larger than a preset minimum collision free distance, the two fibers will be generated in the space. The RVE size is chosen based on results from previous studies for straight fiber RVEs with varying sizes, which suggest that satisfactory results are given when the ratio of RVE side length to the length of fibers is 2:1.

While the industrial applications indicate RaFCs with high AR and VF, the fiber AR in RaFC RVEs are comparatively low in the existed research works. Boehm et al [20] used the RSA method generated a 15% VF RVE with short fibers of AR=5. Tu et al [21] also used RSA approach for fibers of AR=7:1. Pan et al [24] applied the modified RSA algorithm for a RaFC with fiber AR=10:1 and reached RaFC VF=13.5%. For fibers with larger aspect ratio AR=20, the relation between the fiber AR and the achievable fiber VF has been reached to 20% by Evans et al. [28], to 30% by Parkhouse et al. [29], to 18.5% by Toll et al. [30], and to 27% by Williams et al. [15].

In this part of the thesis, all filaments in the RaFC RVE are simulated as spatial straight cylinders with AR=100:1 with aforementioned techniques. Figure 2-8 illustrates a random fiber composite RVE generated with three layers of straight cylindrical fibers of high aspect ratio AR=100:1, and high volume fraction VF=31.8%, which is in the range of the values employed in industry.

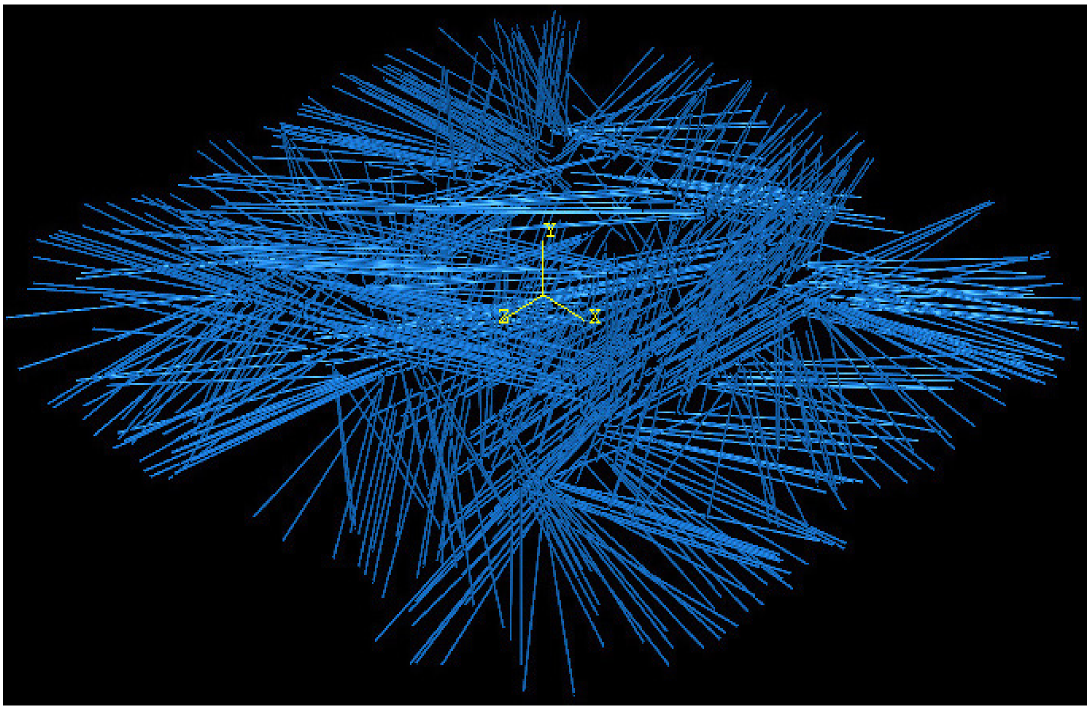

Fig 2-8. A RaFC RVE with AR=100:1; VF=31.8%

Chapter 3

Numerical Simulation of Random Chopped Fiber-Reinforced Composite RaFC material RVEs.

3.1. MATLAB Simulation and Analysis of Multi-Segments RaFC Fiber Geometry.

As presented in the aforementioned introduction, we have reached a random chopped fiber-reinforced composite (RaFC) representative volume element (RVE) model with high fiber aspect ratio (100:1) and high fiber volume fraction number (31.8%). However this RVE model only consists of straight cylinder fibers, which the fiber geometry is not quiet accurate based on the experimental observation on the RaFC material specimen.

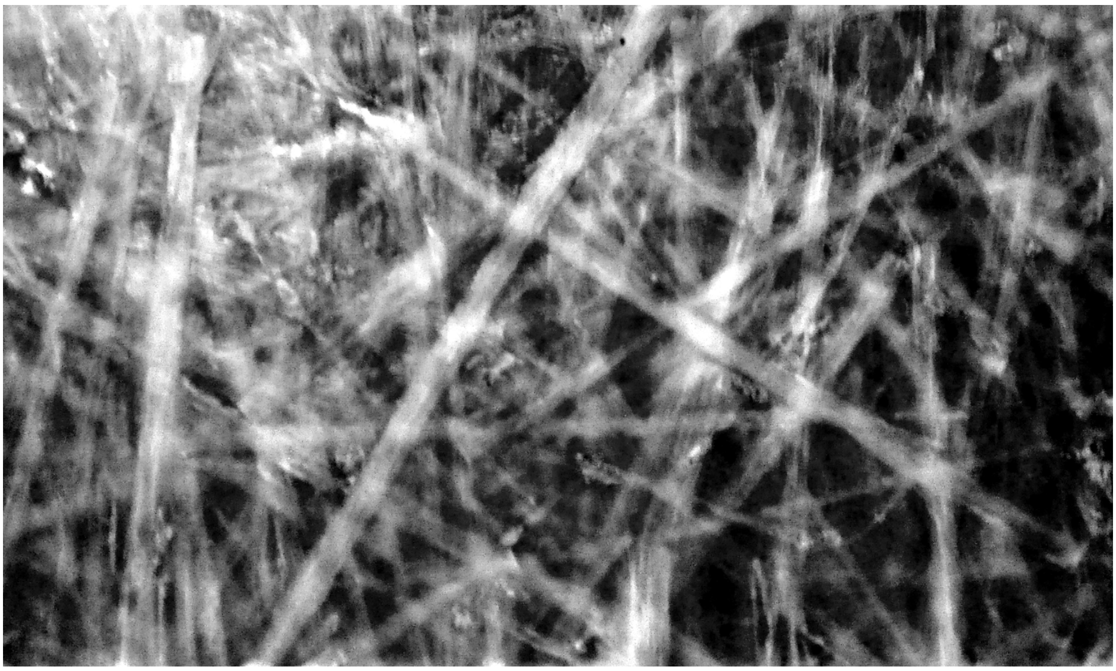

Fig 3-1. Observation of the longitudinal geometries of RaFC fibers.

In Fig 3-1, the microscope figures of the RaFC materials clearly show that the most of the RaFC reinforced fiber longitudinal axes are not straight lines. During the actual RaFC manufacturing process when a new fiber strand is deposited into the material specimen and placed on an existed fiber strand, the newly deposited fiber stand “bands over” in fiber longitudinal/axial direction due to resistance from contacting with the existed fibers underneath.

Based on the previous achieved RVE model, a new RVE with new fiber geometry is proposed by using multiple spatial fiber segments instead of using straight cylindrical fiber geometries. Before translated into ABAQUS PYTHON, the new model is depicted by writing in MATLAB due to its great advantages in matrix manipulation. Evidently, the spatial displacements of fiber segments are much easier to be achieved in MATLAB language than in ABAQUS PYTHON, which the later one is an interpreted language. Several important steps of generating the nulti-spatial fiber segments RVE model are listed as follows.

(1). Same previous steps of numerical modeling of RaFC cylindrical fiber reinforcements RVE.

(2). Apply SSSD algorithm to detect the spatial collisions between cylindrical fibers and calculate the collision point coordinates on two fibers.

(3). When collision happens, instead of getting rid of newly generated cylindrical fiber in the previous model, the collision point coordinates are calculated and this exactly point on the new fiber is “popped out” upwards to form a multi-segments fiber geometry as shown in Fig. 3-2.

(4) As long as a new segment within the fiber is generated, SSSD algorithm detections between this segment and all the previous successfully generated fiber segments are necessarily performed to avoid any spatial collision.

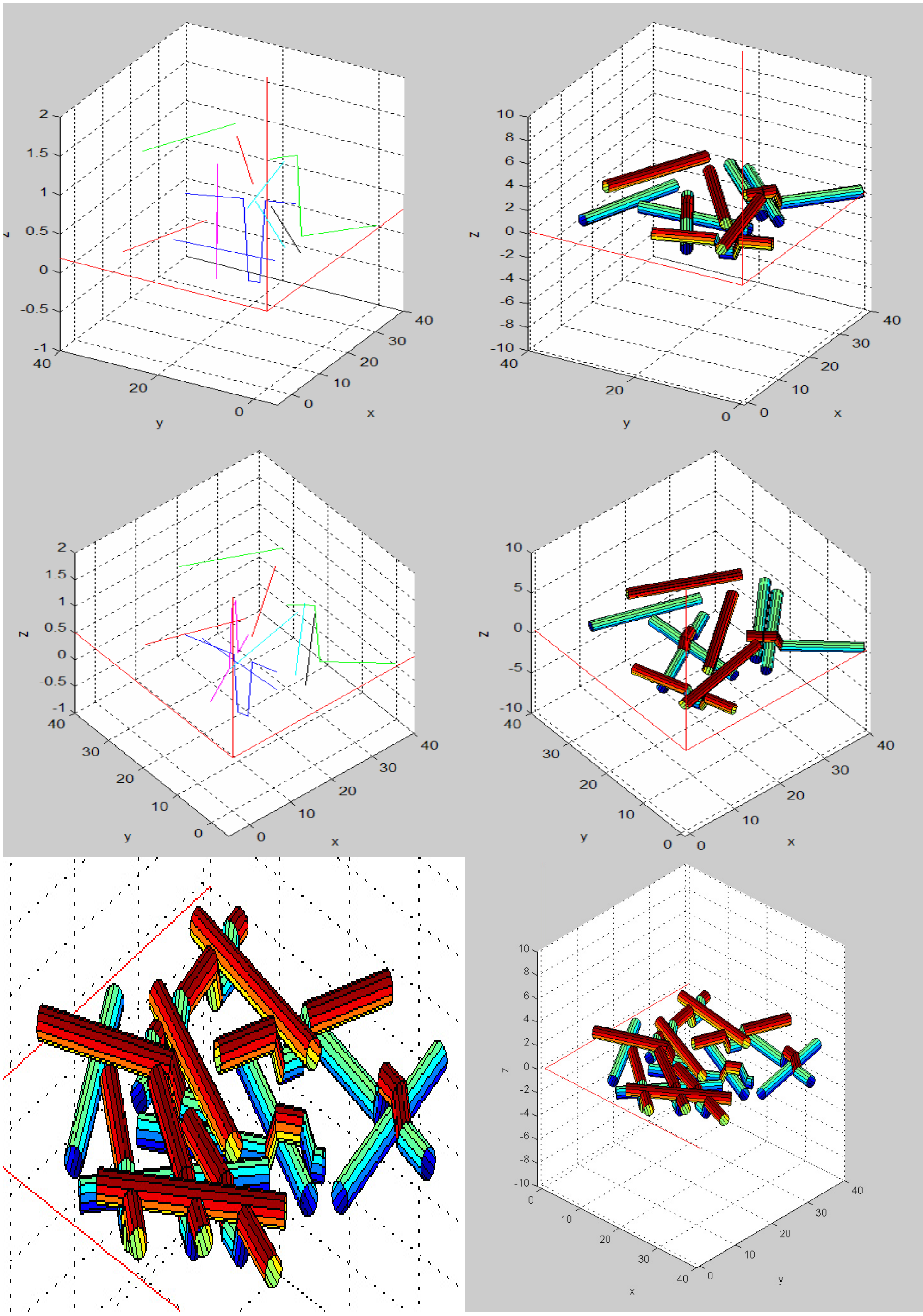

Fig 3-2. The spatial multi-segments fiber geometry described in MATLAB

The step (3) mentioned above is a little bit tricky. By applying the developed SSSD algorithm, one can efficiently find out the collision point (if any) on two fibers. But to change a straight fiber into a “curved” multi-segments one in 3-D space is not that easy, it requires the calculation of spatial coordinates of three fiber line segments’ end points, which involves the spatial rotation matrix and spatial displacement matrix based on the original spatial fiber segments, this can be easily achieved in 2-D, but can be calculation resource consuming and mistakable in 3-D.

To solve this problem, the detail steps in ABAQUS PYTHON to generate a “curved” multi-segments-fiber geometry in space are described as follows:

(1). Generate a straight cylindrical fiber with aspect ratio 100:1 along the z axis.

(2). Apply randomly generated rotation matrix R and displacement matrix D on the fiber.

(3). Apply SSSD algorithm for collision detection, when collision happens, document and translate the collision location into a “ratio” on the fiber. For example: the collision point is at 16.8% ratio on the fiber, counted from end point 1 to end point 2.

(4) Generate a new fiber on the z axis, where there’s a “curved” multi-segments geometry at 16.8% of the fiber counted from original point.

(5) Apply the same rotation matrix R and displacement matrix D on this multi-segments fiber geometry.

Thus the multi-segments geometry of the newly generated fiber is collision free in the 3-D space.

Two major disadvantages of this RaFC RVE model with multi-segments fiber geometry are documented after multiple tests.

First, the multi-segments geometry itself does not vividly describe the real RaFC fibers. Let's call the "curved" part of the fiber an artificial fiber "bridge", we create the fiber "bridge" by detecting collision of the cylindrical fibers, and "pop" the collided region upwards. Every "bridge" consists of three line segments, with two of them in out of plane orientation and one above segment parallel to the main longitudinal fiber direction. When sweeping the fiber geometry in ABAQUS, the cross section geometry remains perpendicular to the sweeping path during the sweeping process. When passing through the junction of the multi-segments, the discontinues of the second derivative which is the sudden change of the sweeping path direction leads to a sharp turn at the junction region, this can be seen clearly in the bottom left corner figure in Fig 3-2. This discontinues feature does not describe the real long continues RaFC materials fiber well, as we can see from the real fiber sample under the microscope bends smoothly at the previously detected collided region.

Second, the efficiency of the algorithm becomes comparatively low while the fiber/segment number is increasing. Since the aspect ratio of one single fiber is defined as more than 100:1 according to the microscope observation, and the RVE side length is two times of the fiber length, every single fiber is more likely "passing through” the whole RVE area and has a great chance to collide with majority of the previous fibers. Thus at the optimization point of view, the 3-D RVE spatial division similar to what have been done to the 2-D unidirectional fibers RVE does not necessarily bring much optimization on the algorithm but simply will be a drawback. Without doubt, no matter the 3-D RVE is spatially divided or not, every single segment in the new generated fiber needs to be run though the SSSD algorithm and to be compared with all previous existed segments in all fibers. When the volume fraction is reaching 40% the segment number is increasing rapidly for every new generated fiber. A statistical example, the 500^{th} generated fiber has 50 segments along its longitudinal direction and every generated segment needs to do 30 times SSSD collision check towards all the previous fiber segments, which is $50 \times 30 \times 500 = 750{,}000$ times SSSD calculations for one single fiber.

For the two reasons mentioned above, in a good RaFC model simulation the 2^{nd} derivative of the points on the fiber longitudinal direction should be continues throughout the whole geometry. As a result of the mentioned geometric flaw, when deciding material properties such as the loading property of the whole RaFC RVE, these sharp turns of the multi-segments fibers geometries may introduce severe local stress concentrations and thus accumulatively influence the accuracy of the simulation work.

3.2. Smooth Curved RaFC Fiber Geometry: Numerical Methods on Fiber Shape Control Points.

By applying the developed SSSD algorithm, we can calculate the spatial collision points' coordinates and derive the control points of a smoothly curved RaFC fiber in 3-D space. Based on the known data which is the collision points coordinates, multi-segments are created to simulate the fiber geometries. The disadvantage of the multi-segments geometry has been discussed, that a better RaFC fiber geometry shape would have the feature of 2nd and lower derivative continuity.

To achieve this better geometry, two types of numerical methods including piecewise cubic polynomial interpolation and the curve fitting are introduced.

3.2.1. Polynomial Interpolation.

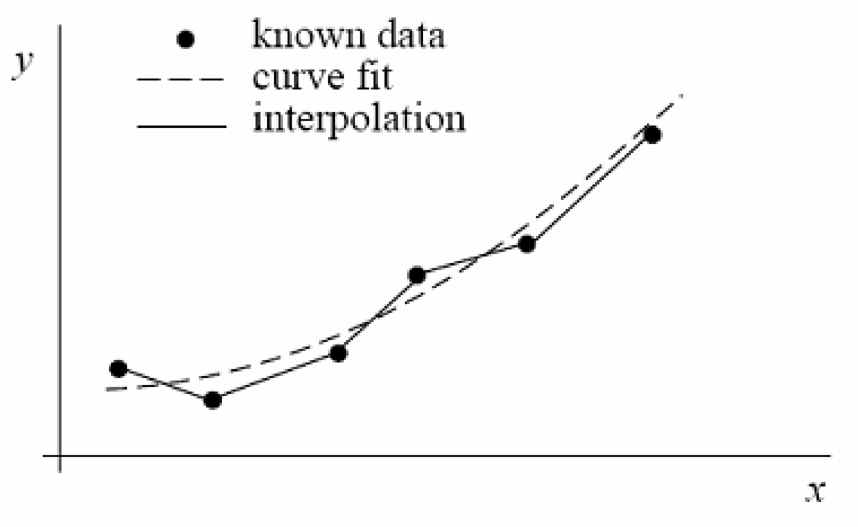

Fig 3-3. Curve fitting and interpolation of the RaFC fiber control points.

As shown in Fig 3-3, the mathematical equivalent of reading between the lines is the interpolation on a fixed set of control points data (x_i, y_i) , $i = 1,\dots,n$, which are calculated by the SSSD algorithm as discrete samples of the hard-to-evaluate RaFC fiber shape function $y = f(x)$. Interpolation on these data involves constructing and then evaluating and interpolating function, or interpolant, $y = F(x)$ at values of $x = \underline{x}$ that may or may not be in the (x_i, y_i) data set. The interpolation function $F(x)$ is determined by requiring that it pass through the control points' data set (x_i, y_i).

Polynomial interpolation of the fiber shape function involves finding the equation of $P_{n-1}(x)$, where

$$P_{n-1}(x) = c_n x^{n-1} + c_{n-1} x^{n-2} + ... + c_2 x + 1 \tag{3-1}$$

which is the unique polynomial of degree n-1 that passes through n known control point data pairs.

3.2.2. Curve Fitting.

When given the set of fiber shape control points $y_i = f(x_i), i = 1,2,...,n$ obtained from SSSD calculation, it is often necessary to evaluate y for x values which are not in the original data set.

In curve fitting, the approximating function passes near the data points, but usually not exactly through them. This feature makes the RaFC fiber geometry more smooth, but also raise the disadvantage that lowering the control precision. Instead of passing right through the control points, the fiber may passes near it and thus creates tiny collision with other spatial fibers.

In contrast to curve fitting, the interpolation function passes exactly through each of the fiber shape control points and thus ensures the 3-D fiber collision-free situation. In our simulation work, in order to form the right accurate fiber geometry we apply the interpolation method on a basic spline which is called cubic B-spline, mathematically described by polynomial functions.

3.3. Smooth Curved RaFC Fiber Geometry: Mathematical Depiction of Splines.

3.3.1. Mathematical Depiction of B-Spline.

In order to obtain a better representation of the true geometry of RaFC continues long fiber, which was previously shown in Fig 2-1, the mathematical description of a smooth cubic B-spline shape with continues second derivative is presented.

In the mathematical field of numerical analysis, a B-spline is a spline function that has minimal support with respect to a given degree, smoothness, and domain partition. The term B-spline was coined by Schoenberg and is the short form for basis spline [38]. A fundamental theorem states that every spline function of a given degree, smoothness, and domain partition can be represented as a linear combination of B-splines of that same degree and smoothness and over that same partition.

Two types of fiber B-splines used in our work to represent RaFC fiber geometry are: uniform B-spline and non-uniform B-spline. A non-uniform fiber B-spline is a curve where the intervals between successive control points is not, or not necessarily equal, which means the knot vector of interior knot spans are not equal. A common form is where intervals are successively reduced, interpolating control points.

Given m real values t_i, called knots, with $t_0 \le t_1 \le \cdots t_{m-1}$, a B-spline of degree n is a parametric curve S, where

$$S:[t_0, t_{m-1}] \to \Re^2 \tag{3-2}$$

where the B-spline S composed of a linear combination of basis B-spline $b_{i,n}$ of degree n:

$$S(t) = \sum_{i=0}^{m-n-2} P_i b_{i,n}(t), t \in [t_n, t_{m-n-1}] \tag{3-3}$$

The P_i here are noted as the control points of the fiber B-spline geometry. Here, there are $m-n-1$ control points and they form a convex hull.

When the knots are equidistant the B-spline is uniform, however in the RaFC RVE the control points of the fiber curves in most cases are not equidistant, thus the geometry we use is said to be non-uniform B-spline.

Two different types of B-splines [38] are used in this thesis to represent the geometry of RaFC fibers.

3.3.2. Mathematical Depiction of Quadratic B-Spline

Quadratic B-splines with uniform knot-vector is the first type of B-spline used in this work. The basis shape function can easily be precalculated, and is equal for each segment. An example of quadratic B-spline shape function is presented as follows:

$$b_{j,2}(t) = \begin{cases} \frac{1}{2}t^2 \\ -t^2 + t + \frac{1}{2} \\ \frac{1}{2}(1-t)^2 \end{cases} \tag{3-4}$$

Transferred into matrix form, we have:

$$S_i(t) = [t^2 \quad t \quad 1]\frac{1}{2}\begin{bmatrix} 1 & -2 & 1 \\ -2 & 2 & 0 \\ 1 & 1 & 0 \end{bmatrix}\begin{bmatrix} P_{i-1} \\ P_i \\ P_{i+1} \end{bmatrix} \text{ for } t \in [0,1], i = 1,2...m-2 \tag{3-5}$$

3.3.3. Mathematical Depiction of Cubic B-Spline

In order to have full control of the fiber geometry shape, the most commonly used B-spline type in this research work is Cubic B-spline.

A Cubic B-spline formulation for a single segment can be written as:

$$S_i(t) = \sum_{k=0}^{3} P_{i-3+k} b_{i-3+k,3}(t)\,; \quad t \in [0,1] \tag{3-6}$$

where S_i is the ith B-spline segment and P is the set of control points of the RaFC fiber geometry, segment i and k is the local control point index.

A set of fiber control points would be:

$$P_i^w = (w_i x_i, w_i y_i, w_i z_i, w_i) \tag{3-7}$$

where the w_i is a very important variable defined as the weight of the fiber. The weight is pulling the fiber curve towards control point P_i as it increases or moving the fiber curve away as it decreases.

In conclusion, an entire set of segments, $m-2$ fiber curves $(S_3 S_4 ... S_m)$ defined by

$m+1$ control points $(P_0, P_1, \ldots, P_m, m \geq 3)$, as one B-spline would be defined as:

$$S(t) = \sum_{i=0}^{m-1} P_i b_{i,3}(t) \tag{3-8}$$

where i is the control point number and t is a global parameter giving knot values. The above equation expresses a cubic B-spline curve as a linear combination of B-spline basis shape functions.

Here is an example of a cubic B-spline applied as RaFC fiber geometry:

$$S_i(t) = [t^3 \quad t^2 \quad t \quad 1]\frac{1}{6}\begin{bmatrix} -1 & 3 & -3 & 1 \\ 3 & -6 & 3 & 0 \\ -3 & 0 & 3 & 0 \\ 1 & 4 & 1 & 0 \end{bmatrix}\begin{bmatrix} P_{i-1} \\ P_i \\ P_{i+1} \\ P_{i+2} \end{bmatrix} \quad \text{for} \quad t \in [0,1] \tag{3-9}$$

3.4. Smooth Curved RaFC Fiber Geometry: Cubic B-Spline Polynomial Interpolation

Based on the introduced cubic B-spline and polynomial interpolation methods, a smooth curved RaFC fiber geometry can be obtained and its shape is controllable by manipulating and changing the shape function variables.

The cubic B-spline interpolation is explained by the example below.

Given five fiber shape control points data pairs: (0, 5.1765), (0.375, 61.1683), (0.75, 14.7059), (1.125, 6.4824), (1.5, -2.8103), to construct four cubic polynomial lines through these five control points:

$$P_i(x) = a_i + b_i(x - x_i) + c_i(x - x_i)^2 + d_i(x - x_i)^3, \quad i = 1,2,3,4 \tag{3-10}$$

whose $P_i(x), P_i'(x), P_i''(x)$ are all continuous. The interpolation of the fiber control points is shown in Fig 3-4 as below.

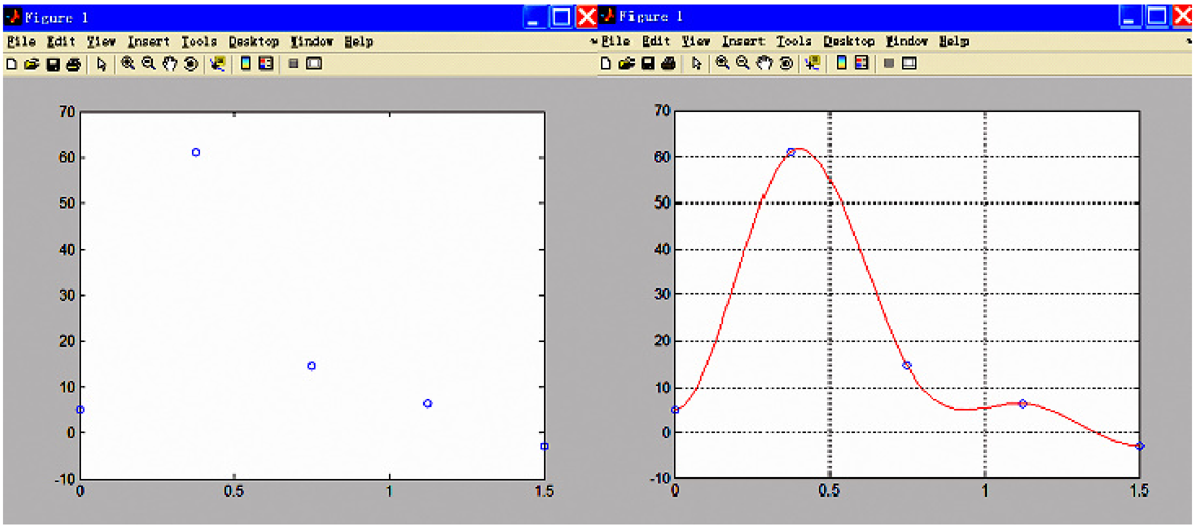

Fig 3-4. A cubic B-spline polynomial interpolation of 5 control points

There are five control points on this cubic B-spline. On each control point, the $P_i(x), P_i'(x), P_i''(x)$ are continuous. The continuity of the 2nd derivative $P_i''(x)$ has the effect of coupling and smoothing the adjacent piecewise cubic polynomials, that is, the fiber geometry shape.

As shown in Fig 3-5, $n-2$ equations are computed if there are n control points.

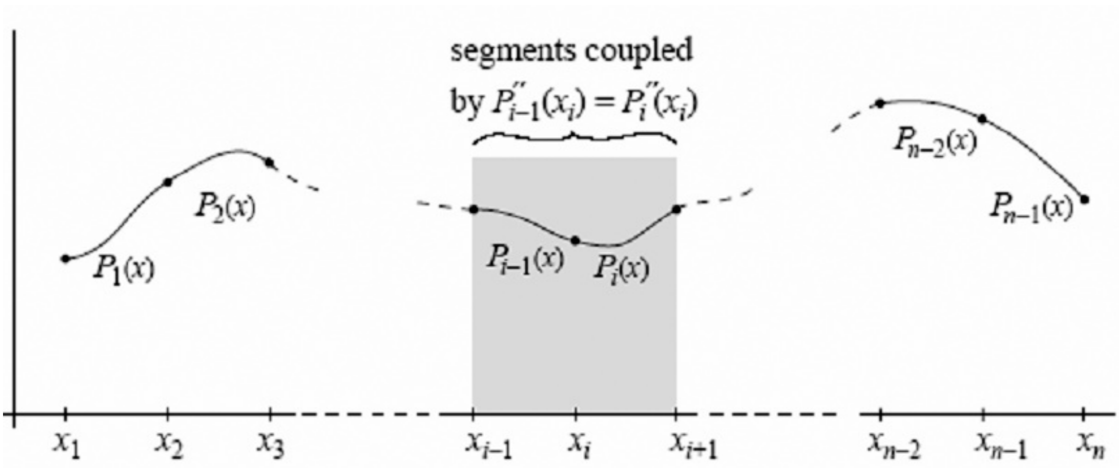

Fig 3-5. A cubic B-spline polynomial interpolation of n control points

The RaFC fibers are at the aspect ratio of more than 100:1. For each fiber, it is possible to reach 20 or more control points. When reaching high number of control points, the cubic spline interpolation is broken into piecewise since its computational efficiency is higher than using a single “high degree polynomial function” to describe the whole curved spline.

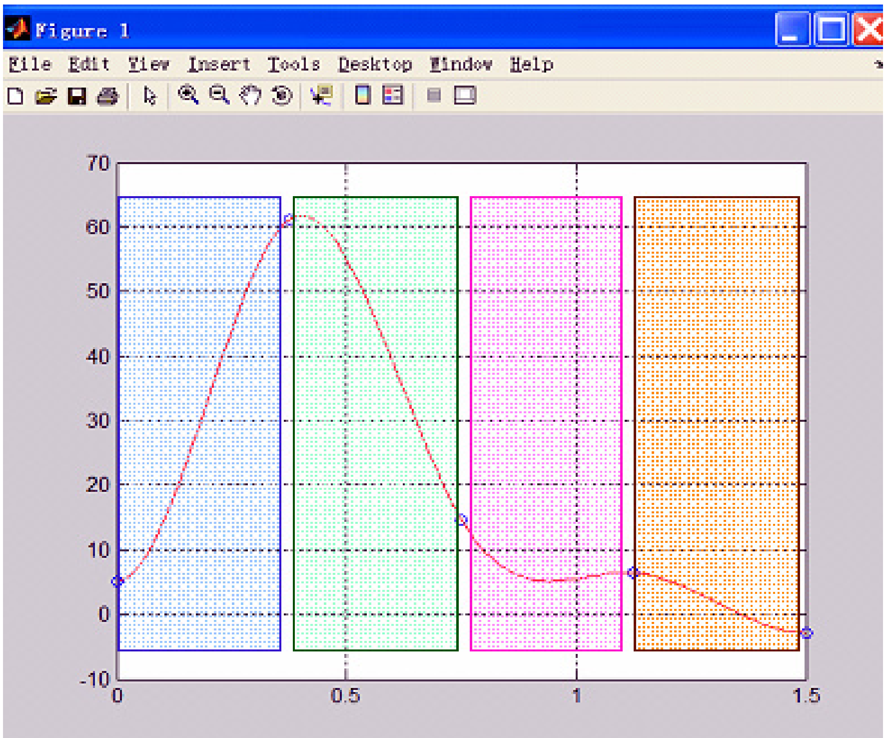

Fig 3-6. A piecewise cubic B-spline polynomial interpolation of 5 control points

The cubic B-spline shape example in Fig 3-4 is broke into piecewise expression.

$$P_i(x) = a_i + b_i(x - x_i) + c_i(x - x_i)^2 + d_i(x - x_i)^3\,,\quad i = 1,2,3,4 \tag{3-11}$$

transformed into detailed piecewise forms:

$$P_1(x) = 5.18 + 61.17(x - 0.375) + 14.71(x - 0.375)^2 + 6.48(x - 0.375)^3 \tag{3-12}$$

$$P_2(x) = 49.17(x - 0.75) - 120.43(x - 0.75)^2 - 4.92(x - 0.75)^3 \tag{3-13}$$

$$P_3(x) = 1063.38 - 932.27(x - 1.125) + 480(x - 1.125)^2 - 171.98(x - 1.125)^3 \tag{3-14}$$

$$P_4(x) = -1773.91 + 1255.35(x - 1.5) - 579.54(x - 1.5)^2 + 317.42(x - 1.5)^3 \tag{3-15}$$

The piecewise expression of the cubic B-spline shape is shown in Fig 3-6. Fig 3-7 shows different interpolation methods applying on same previously used data sets.

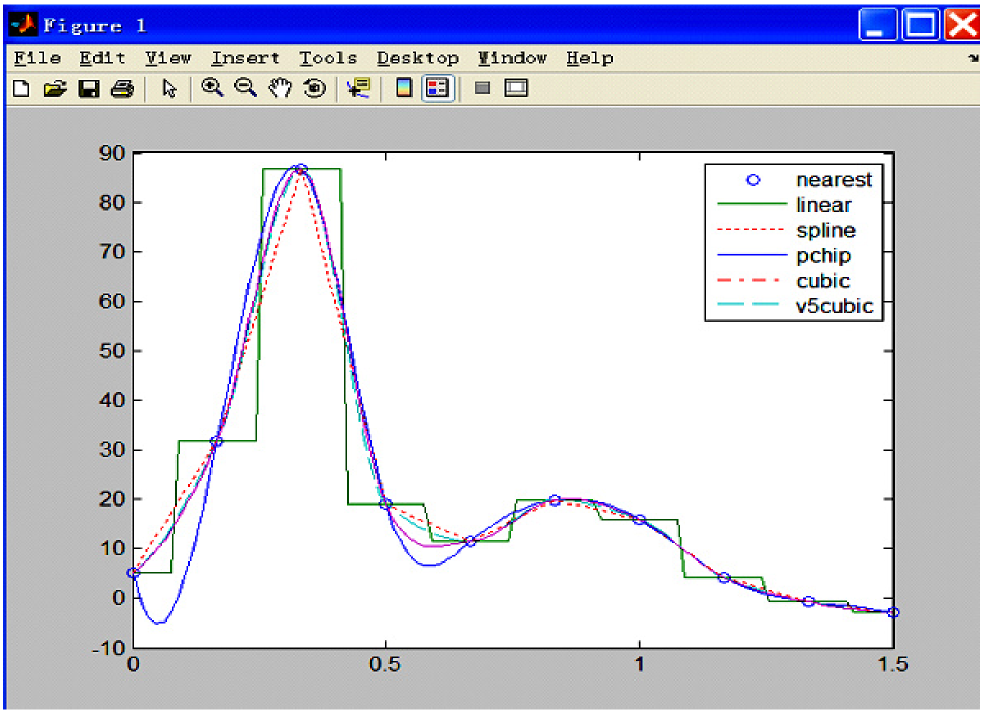

Fig 3-7. Different cubic B-spline polynomial interpolation methods effects.

3.5. ABAQUS PYTHON Simulation of Smooth Curved RaFC Fiber Geometry using Cubic B-Spline Polynomial Interpolation

As mentioned in the previous introduction, the cubic B-spline obtained by polynomial interpolation method has very good features, that its 2nd and lower derivative continuity and in the form of piecewise cubic polynomial, which is a good representation of the smooth curved RaFC fiber geometry.

Combined the aforementioned numerical methods and techniques with the developed SSSD algorithm and implanted into ABAQUS with PYTHON language programming, we propose a more accurate RaFC RVE model which is a simulation of the real material specimens.

Fig 3-8 shows a polynomial interpolation cubic B-spline shape RaFC fiber sweeping path obtained in ABAQUS PYTHON.

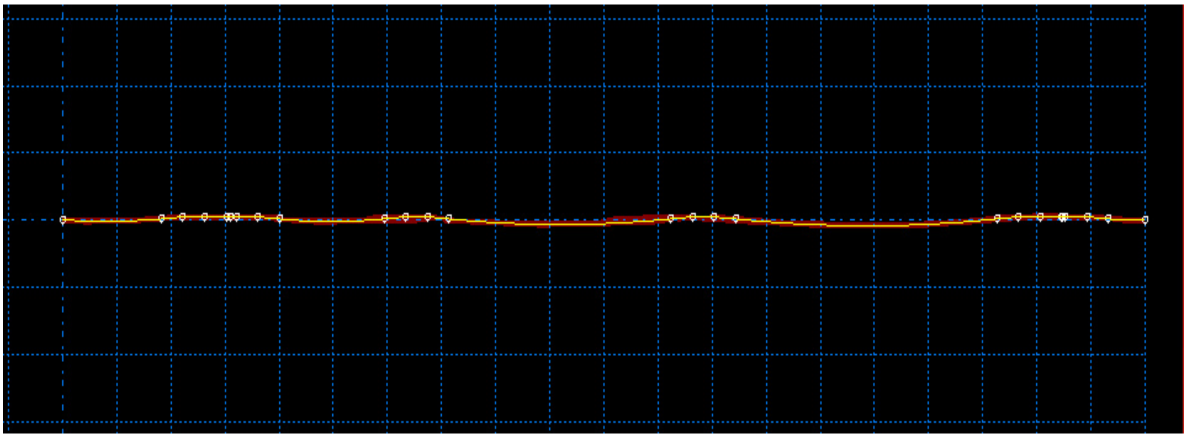

Fig 3-8. A polynomial interpolation cubic B-spline shape RaFC fiber sweeping path by ABAQUS PYTHON.

Fig 3-9 and Fig 3-10 shows the actual curved fiber geometry by ABAQUS PYTHON. Note the cross section of the fiber here is still circular shape.

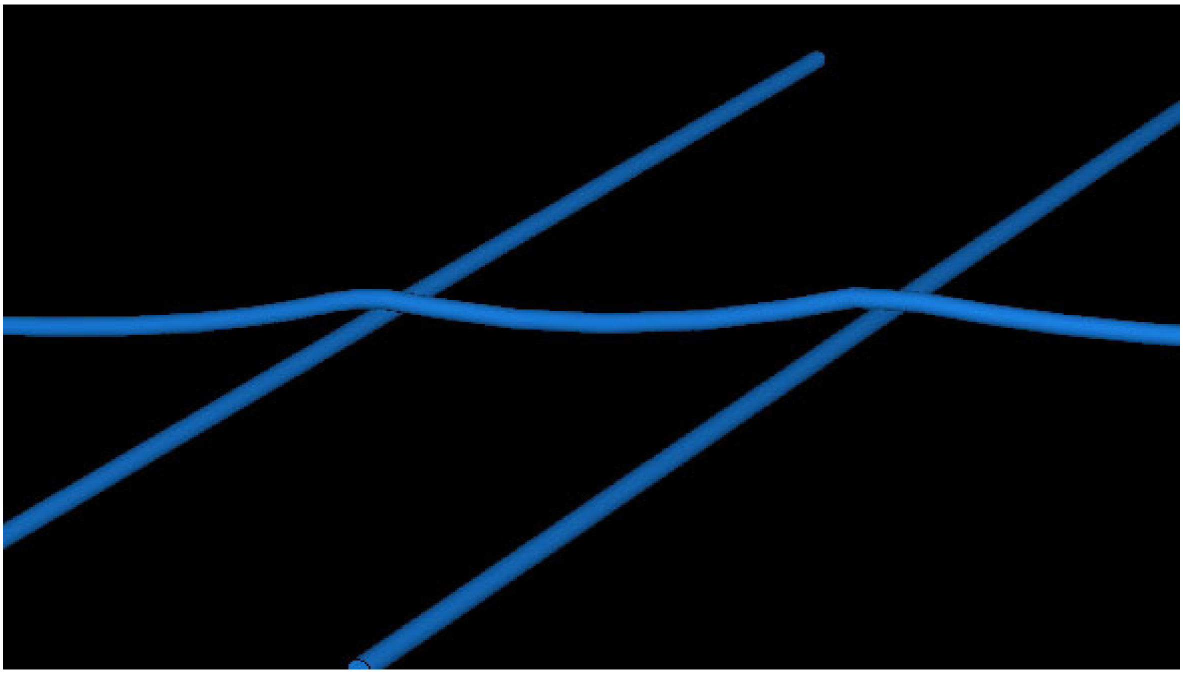

Fig 3-9. An actual curved cubic B-spline fiber geometry by ABAQUS PYTHON

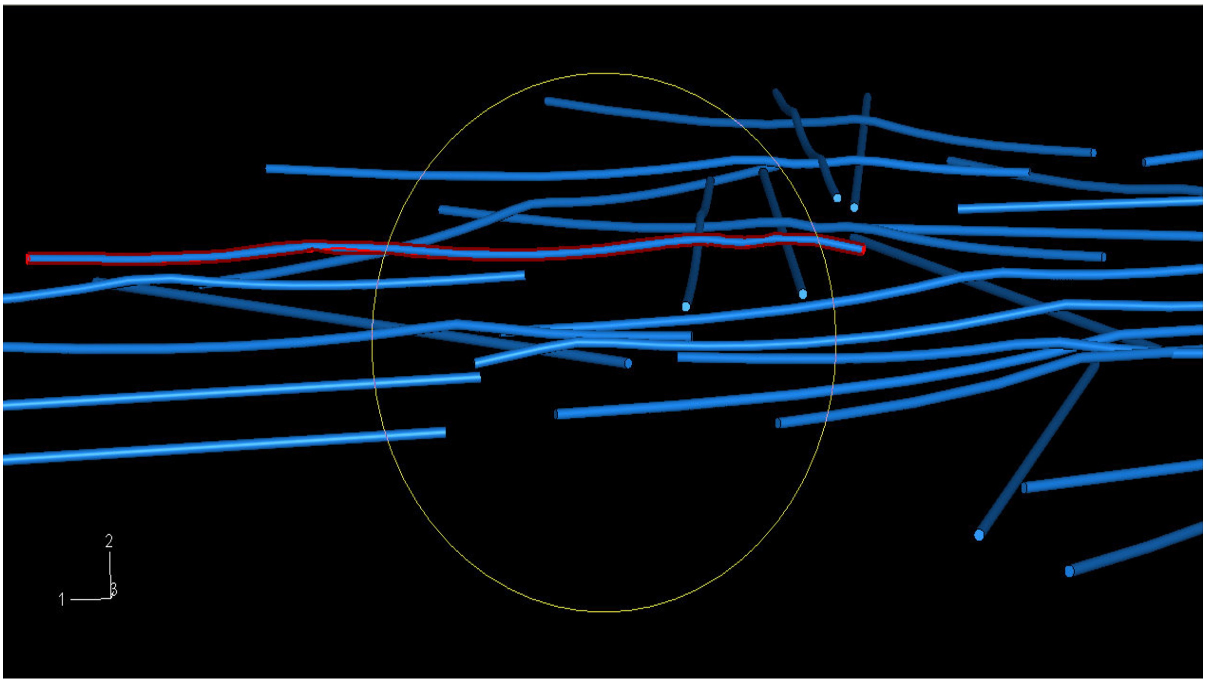

Fig 3-10. An actual curved cubic B-spline fiber geometry by ABAQUS PYTHON

For fiber cross sectional geometry, instead of circular shape cross section, the elliptical cross-sectional fiber strands are applied in the RVE, as shown in Fig 3-11. The real cross sectional geometries of the RaFC material fiber strands are ribbon shape and the cross section geometry was presented in Fig 2-5 in the previous part of the thesis.

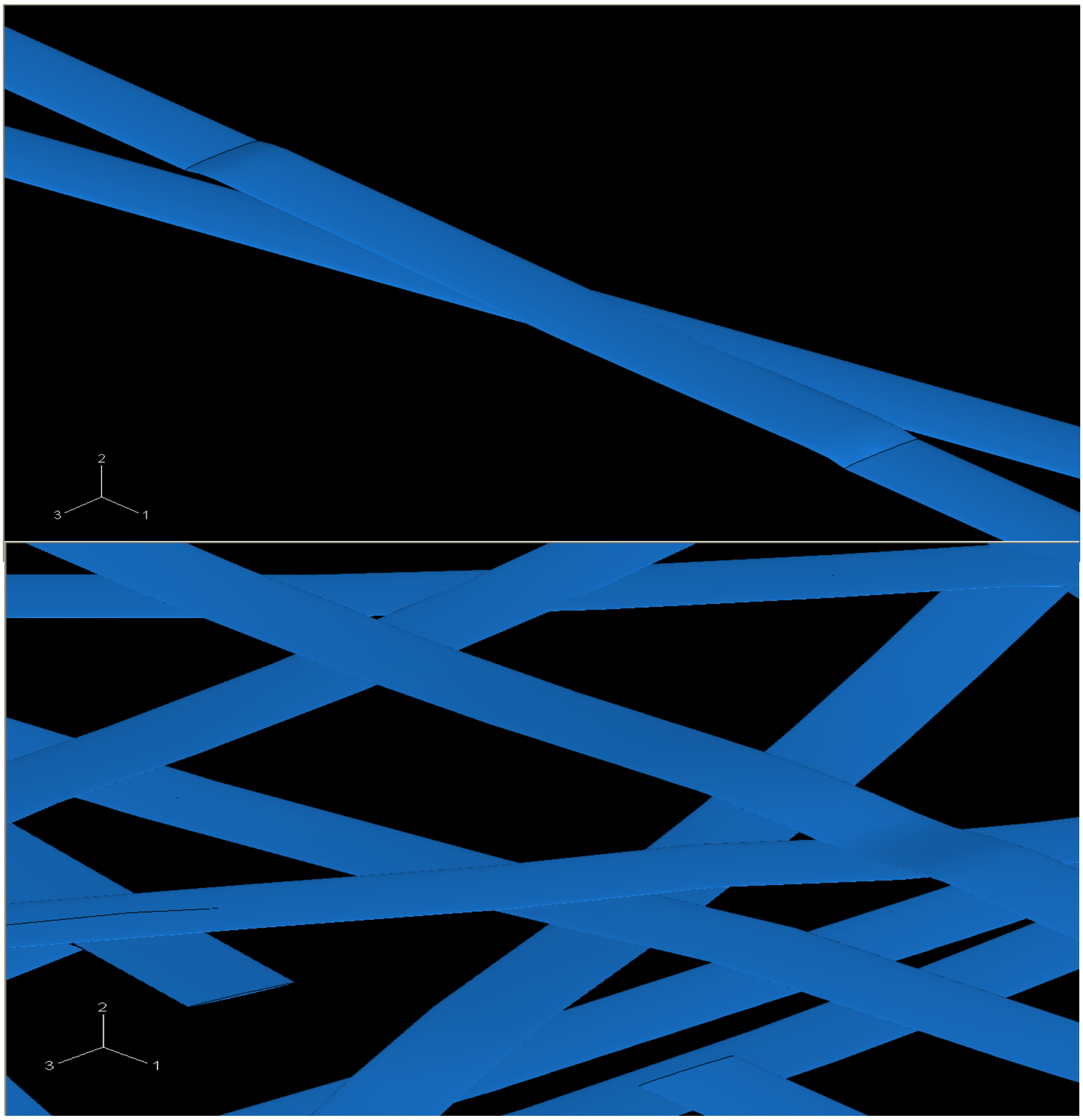

Fig 3-11. Elliptical cross sectional curved fiber geometry in ABAQUS PYTHON

Shown in Fig 3-12, a RaFC RVE with the accurate curved fiber geometry is obtained in ABAQUS PYTHON, the volume fraction reached 40% and the aspect ratio is 3333:1 for each single fiber filament.

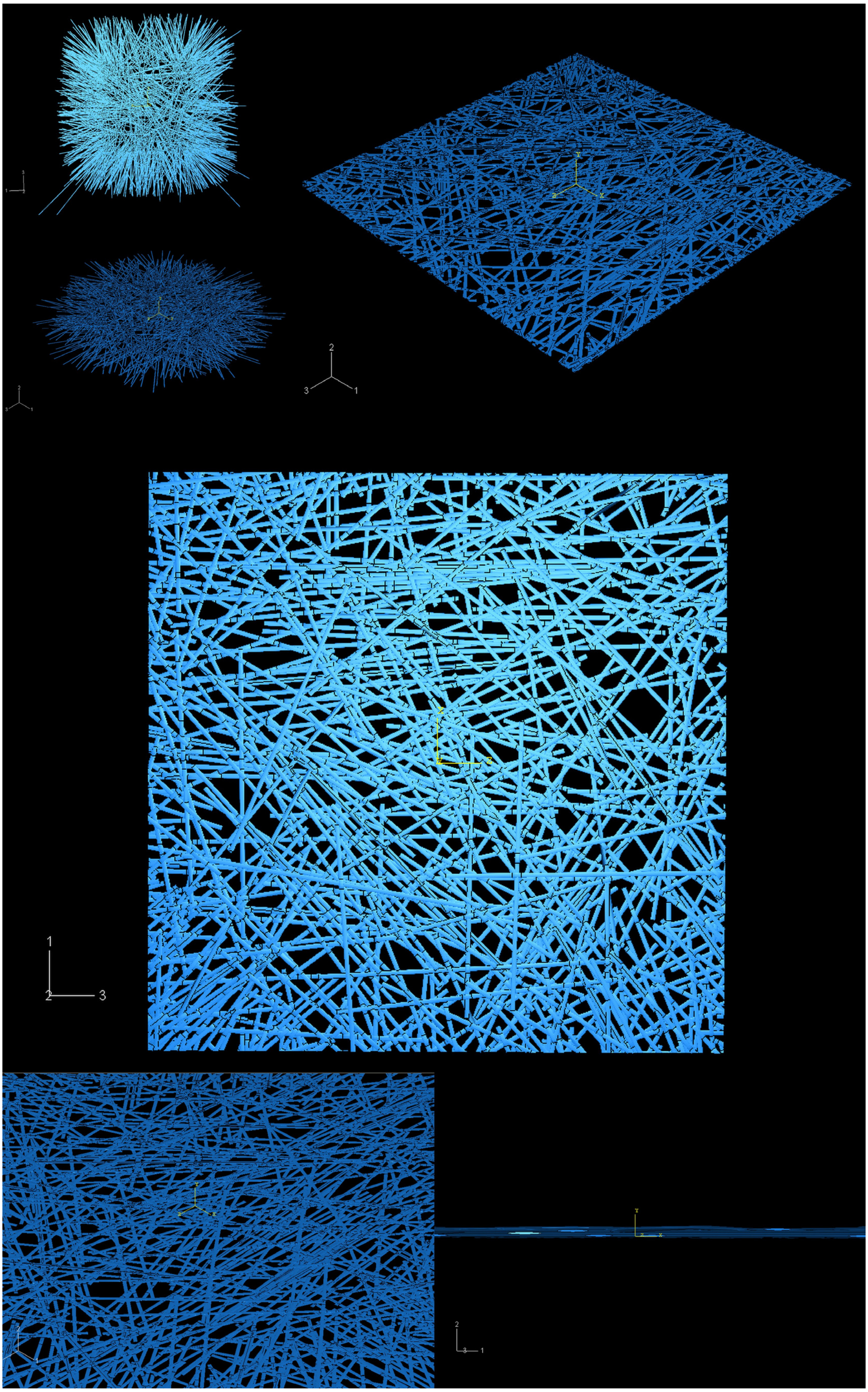

Fig 3-12. A RaFC RVE with fiber AR=3333:1, RVE VF=40.29% and elliptical c/s ribbon shaped smooth curved fiber geometry by ABAQUS PYTHON

Chapter 4
Conclusion

By experimental observation and PYTHON programming, unidirectional RaFC fiber strands RVEs are generated automatically in ABAQUS. When the cross sectional aspect ratios of the second phase reinforced fiber reinforcements are not necessarily one, different types of RVE models with various cross sectional shapes fibers are simulated automatically. The fiber volume fraction number of the unidirectional RVE reached up to 70%. By applying a RSA algorithm and based on the developed SSSD algorithm with modified LU decomposition numerical method, a 3-Dimentional RaFC material RVE model is simulated in ABAQUS PYTHON with straight random distribution and orientation fibers of high fiber aspect ratio AR=100:1 and with high volume fraction number VF>31.8%.

By modifying the SSSD algorithm, the multi-segments fiber geometries are obtained in MATLAB environment. Quadratic and cubic polynomial B-spline interpolation and the curve fitting numerical methods are applied to the fiber shape control points which are calculated by the developed SSSD algorithm. Based on the multi-segments fiber geometries and aforementioned techniques, smooth curved fiber geometries depicted by cubic B-spline polynomial interpolation are obtained and different types of RaFC RVEs with high fiber aspect ratio up to 3333:1 and high volume fraction number up to 40.29% are simulated in ABAQUS by PYTHON language programming.

This simulation work is a good support for the future discovery of mechanical properties of random chopped fiber reinforced composites RaFC materials.

References

[1] Harris, C.E., Starnes, J.H., and Shuart, M.J., 2002, “Design and Manufacturing of Aerospace Composite Structures, State-of-the-art Assessment,” J. Aircraft, 39, pp. 545-560.

[2] Soutis, C., 2005, “Carbon Fiber Reinforced Plastics in Aircraft Applications,” Materials Science and Engineering. A, 412(1-2), pp. 171-176.

[3] Riegner, D.A., 1983, “Composites in the Automotive Industry,” ASTM Standardization News.

[4] Beardmore, P., 1986, “Composite Structures for Automobiles,” Composite Structures, 5, pp. 163-176.

[5] Daniel, I.M., Ishai, O., 1994, “Engineering Mechanics of Composite Materials,” Oxford University Press.

[6] Mackerle, J., 2004, “Finite Element Analyses and Simulations of Manufacturing Processes of Composites and Their Mechanical Properties, a Bibliography (1985–2003),” Computational Materials Science, 31(3-4), pp. 187-219.

[7] Jacob, G.C., Starbuck, J.M., Fellers, J.F., Simunovic, S., Boeman, R.G., 2006, “Fracture Toughness in Random-Chopped Fiber-Reinforced Composites and Their Strain Rate Dependence,” Journal of Applied Polymer Science, 100(1), pp. 695-701.

[8] Jacob, G.C., Starbuck, J.M., Fellers, J.F., Simunovic, S., Boeman, R.G., 2006, “Crashworthiness of Various Random Chopped Carbon Fiber Reinforced Epoxy Composite Materials and their Strain Rate Dependence,” Journal of Applied Polymer

Science, 101(3), pp. 1477–1486.

[9] Mallick, P.K., 2007, “Fiber-Reinforced Composites: Materials, Manufacturing, and Design, 3rd Ed,” CRC Press.

[10] Brady, G., Clauser, H., Vaccari, J., 1997, “Materials Handbook, 15th Ed.” McGraw-Hill Press.

[11] Cendre, E., “Characterization of Glass-Fiber Polymer Composites using X-Ray Synchrotron Micro-Tomography,” Report, Materials Research Department, Risø National Laboratory, Roskilde, Denmark.

[12] Fang, Y., 2006, “Influence of Glass Fiber Diameter on the Strength of Fiber and Composite,” Journal of Fiber Glass, 06, pp. 01-07.

[13] Caizzo, A.A., Constanzo, F., 2000, “On the Constitutive Relations of Materials with Evolving Microstructure due to Microcracking,” International Journal of Solids and Structures, 37(24), pp. 3375–3398.

[14] Quek, S.C., Waas, A., Shahwan, K.W., Agaram, V., 2004, “Compressive Response and Failure of Braided Textile Composite: Part 2-Computations,” International Journal of Non-Linear Mechanics, 39(4), pp. 649–663.

[15] Williams, S.R., Philipse, A.P., “Random Packings of Spheres and Spherocylinders Simulated by Mechanical Contraction,” Physical Review E. 67(5).

[16] Hinrichsen, E., Feder, J., Joessang, T., 1990, “Random Packing of Discs in Two Dimensions,” Physical Review A, 41, pp. 4199-4209.

[17] Gusev, A.A., 1997, “Representative Volume Element Size for Elastic Composites: a Numerical Study,” Journal of Mechanics and Physics of Solids, 45, pp. 1449-1459.

[18] Gusev, A.A., Heggli, M., Lusti, H.R., Hine, P.J., 2002, "Orientation Averaging for Stiffness and Thermal Expansion of Short Fiber Composites," Advanced Engineering Materials, 4(12), pp. 927-931.

[19] Gusev, A.A., Hine, P.J., Ward, I.M., 2000, "Fiber Packing and Elastic Properties of a Transversely Random Unidirectional Glass/Epoxy Composite," Composites Science and Technology, 60(4), pp. 535-541.

[20] Boehm, H.J., Eckschlager, A., Han, W., 2002, "Multi-Inclusion Unit Cell Models for Metal Matrix Composites with Randomly Oriented Discontinuous Reinforcements," Computational Material Science, 25(1-2), pp. 42–53.

[21] Tu, S.T., Cai, W.Z., Yin, Y., Ling, X., 2005, "Numerical Simulation of Saturation Behavior of Physical Properties in Composites with Randomly Distributed Second-Phase," Journal of Composite Materials, 39(7), pp. 617-631.

[22] Coelho, D., Thovert, J.F., Adler, P.M., 1997, "Geometrical and Transport Properties of Random Packings of Spheres and Asperical Particles," Physical Review E, 55(2), pp. 1959-1978.

[23] Pan, Y., Iorga, L., Pelegri, A.A., 2007, "Analysis of 3D Random Chopped Fiber Reinforced Composites using FEM and Random Sequential Adsorption," Computational Material Science, 43(3), pp. 450-461.

[24] Widom, B., 1966, "Random Sequential Addition of Hard Sphere to a Volume," Journal of Chemical Physics, 44(10), pp. 3888-3894.

[25] Kari, S., Berger, H., Gabbert, U., 2007, "Numerical Evaluation of Effective Material Properties of Randomly Distributed Short Cylindrical Fibre Composites,"

Computational Material Science, 39(1), pp. 198–204.

[26] Redenbach, C., Vecchio, I., 2011, "Statistical Analysis and Stochastic Modeling of Fibre Composites," Composites Science and Technology, 71(2), pp. 107-112.

[27] Faessel, M., Delisée, C., Bos, F., Castéra, P., 2005, "3D Modeling of Random Cellulosic Fibrous Networks based on X-Ray Tomography and Image Analysis," Composites Science and Technology, 65(13), pp. 1931-1940.

[28] Evans, K.E., Gibson, A.G., 1986, "Prediction of the Maximum Packing Fraction Achievable in Randomly Orientated Short-Fibre Composites," Composites Science and Technology, 25(2), pp. 149-162.

[29] Parkhouse, J.G., Kelly, A., 1995, "The Random Packing of Fibers in Three Dimensions," Mathematical Physical and Engineering Sciences, 451(1943), pp. 737-746.

[30] Toll, S., 1998, "Packing Mechanics of Fiber Reinforcements," Polymer Engineering and Science, 38(8), pp.1337-1350.

[31] Berger, L., 2007, Personal Communication, General Motors.

[32] Feder, J., 1980, "Random Sequential Adsorption," Journal of Theoretical Biology, 87(2), pp. 237-254.

[33] Jones, B.F., 1971, "Further Observations Concerning the Effect of Diameter on the Fracture Strength and Young's Modulus of Carbon and Graphite Fibres Made from Polyacrylonitrile," Journal of Materials Science, 6(9), pp. 1225-1227.

[34] Ramsteiner, F., Theysohn, R., 1985, "The Influence of Fibre Diameter on the Tensile Behavior of Short-Glass-Fibre Reinforced Polymers," Composites Science

and Technology, 24(3), pp. 231-240.

[35] Miwa, M., Horiba, N., "Effects of Fibre Length on Tensile Strength of Carbon/Glass Fibre Hybrid Composites," Journal of Materials Science, 29(4), pp. 973-977.

[36] Zhao, Y.H, Weng, G.J., 1990, "Effective Elastic Moduli of Ribbon-Reinforced Composites," Journal of Applied Mechanics, 57(1), pp. 158-167.

[37] Carl de Boor. A Practical Guide to Splines. Springer-Verlag. 1978: 113-114.

[38] ABAQUS User's Manual, Version 6.6. RI: ABAQUS Inc.; 2006.

[39] PYTHON in a Nutshell, A Desktop Quick Reference. O'Reilly Media, Inc.; 2006.